

1 **Aqueous phase oligomerization of methyl vinyl ketone** 2 **through photooxidation**

3 **Part 2: Development of the chemical mechanism and** 4 **atmospheric implications**

5
6 **Barbara Ervens^{1,2}, Pascal Renard³, Sabine Tlili³, Sylvain Ravier³, Jean-Louis**
7 **Clément⁴, and Anne Monod³**

8 [1] Cooperative Institute for Research in Environmental Sciences, University of Colorado,
9 Boulder, Colorado.

10 [2] Chemical Sciences Division, NOAA Earth System Research Laboratory, Boulder, Colorado.

11 [3] Aix Marseille Université, CNRS, LCE FRE 3416, 13331, Marseille, France

12 [4] Aix Marseille Université, CNRS, ICR UMR7273, 13397, Marseille, France

13
14 Correspondence to: B. Ervens (barbara.ervens@noaa.gov)

15 16 **Abstract**

17 Laboratory experiments of efficient oligomerization from methyl vinyl ketone (MVK) in
18 the bulk aqueous phase were simulated in a box model. Kinetic data are applied (if known) or
19 fitted to the observed MVK decay and oligomer mass increase. Upon model sensitivity studies,
20 in which unconstrained rate constants were varied over several orders of magnitude, a set of
21 reaction parameters was found that could reproduce laboratory data over a wide range of
22 experimental conditions. This mechanism is the first that comprehensively describes such
23 radical-initiated oligomer formation.

24 This mechanism was implemented into a multiphase box model that simulates SOA
25 formation from isoprene, as a precursor of MVK and methacrolein (MACR) in the aqueous and
26 gas phases. While in laboratory experiments oxygen limitation might occur and lead to

1 accelerated oligomer formation, such conditions are likely not met in the atmosphere. The
2 comparison of predicted oligomer formation shows that MVK and MACR likely do negligibly
3 contribute to total SOA as their solubility are low and even reduced in aerosol water due to ionic
4 strength effects (Setchenov coefficients). Significant contribution by oligomers to total SOA (>
5 20%) might occur if a substantial fraction of particulate carbon acts as oligomer precursors
6 and/or if oxygen solubility in aerosol water is strongly reduced due to salting-out effects.

7 **1 Introduction**

8 Organic aerosol particles in the atmosphere comprise about 50% of the total particulate
9 matter mass (Zhang et al., 2007). A small fraction of them are emitted directly by various
10 sources (primary organic aerosol, POA); the major portion is formed by chemical and/or physical
11 processes during their residence time in the atmosphere (secondary organic aerosol, SOA)
12 (Kanakidou et al., 2005). Traditionally, it has been assumed that SOA is formed by condensation
13 of low-volatility or semivolatile organic products that represent gas phase oxidation products
14 from emitted precursor compounds. SOA formation from such products (termed 'gasSOA' by
15 Ervens et al. (2011) since the chemical reactions leading to condensable species occur in the gas
16 phase) is often described by the two-product model (Odum et al., 1996) or, more recently, by the
17 volatility basis set (VBS) (e.g., Donahue et al., 2006; 2011; Trump and Donahue, 2014). While
18 this concept can explain a large amount of observed ambient SOA mass, specific SOA properties
19 (e.g. high oxygen-to-carbon (O/C) ratio) and individual compounds, e.g., dicarboxylic acids,
20 oligomers, cannot be predicted.

21 Several recent laboratory, field and model studies point to efficient chemical reactions in the
22 aqueous phase of cloud/fog droplets and aerosol particles, which lead to low-volatility products
23 that remain in the particle phase upon water evaporation ('aqSOA', Ervens et al., 2011).
24 However, the contribution of aqSOA to total ambient SOA loading has not been quantified yet
25 due to the poor mechanistic understanding, which makes a comprehensive implementation in
26 models difficult and ambiguous. Systematic laboratory experiments have been performed in
27 order to elucidate the SOA formation potential of individual precursors such as small carbonyl
28 compounds (Lim et al., 2010; Noziere et al., 2010; Ervens et al., 2011 and references therein).

29 Several laboratory experiments focused on SOA precursors that are formed from isoprene
30 (Kroll et al., 2005; Altieri et al., 2006; Kroll et al., 2006; Kuwata et al., 2015). Isoprene emission

1 rates exceed those of all other anthropogenic and biogenic organics, and, thus even a small yield
2 (< 5%) might significantly contribute to the total SOA burden (Carlton et al., 2009). Isoprene has
3 a low water-solubility ($K_{H, \text{isoprene}} = 0.013 \text{ M atm}^{-1}$ (Mackay and Shiu, 1981)) and, thus, its
4 fraction in the atmospheric aqueous phases is < 0.001%, related to the total atmospheric isoprene
5 concentration. Its first-generation oxidation products, methyl vinyl ketone (MVK) and
6 methacrolein (MACR), are more soluble ($K_{H, \text{MACR}} = 6.5 \text{ M atm}^{-1}$; $K_{H, \text{MVK}} = 41 \text{ M atm}^{-1}$ (Iraci et
7 al., 1999)), but, yet, their aqueous phase fractions in pure water is < 1%. However, simultaneous
8 measurements of similar small carbonyl compounds in the gas and particle phases have shown
9 that a substantial fraction of them might be associated with the particulate phase (Baboukas et
10 al., 2000; Matsunaga et al., 2005; Healy et al., 2008; Kampf et al., 2013; Kawamura et al., 2013)
11 and thus accumulate in aerosol water. Solubility in non-ideal solutions has often been
12 parameterized by the Setchenov coefficient that predicts salting-in or -out effects, depending on
13 the chemical structure and concentration of the compound (Paasivirta et al., 1999; Wang et al.,
14 2014).

15 Several recent laboratory studies have explored the reactivity of MVK and MACR in the
16 aqueous phase, and depending on the initial concentration, efficient formation of oligomeric
17 compounds has been observed (Zhang et al., 2010; Renard et al., 2013). Organics with
18 oligomeric (or polymeric) structures have also been identified in other laboratory experiments
19 (Kalberer et al., 2004; Tolocka et al., 2004) and ambient aerosol particles (Denkenberger et al.,
20 2007; Polidori et al., 2008; Mazzoleni et al., 2010; Zhang and Ying, 2011) as well as in rainwater
21 (Altieri et al., 2009; Mead et al., 2013; Mead et al., 2015). However, to date the explicit chemical
22 pathways leading to oligomers are not fully implemented into atmospheric chemistry models
23 since the chemical mechanisms are not available. The current study aims at contributing to close
24 this gap by presenting the kinetic and mechanistic details of chemical pathways to explain the
25 observed oligomer formation from MVK during the bulk aqueous phase experiments that were
26 presented by Renard et al. (2013), and in the companion paper of this study (Renard et al., 2015,
27 referred to as 'Part I' hereafter). By fitting kinetic rate constants and combining them with known
28 constants for basic chemical processes, a comprehensive chemical mechanism for the
29 oligomerization of MVK in the aqueous phase is derived (Section 2). This mechanism is used in
30 a multiphase box model and sensitivities of the oligomerization rate to physicochemical
31 parameters (solubility of MVK and oxygen, initial concentration of other potential oligomer

1 precursors) are explored (Section 3). Finally, the question is explored under what atmospheric
2 conditions aqSOA formation from isoprene might be of importance as compared to gasSOA
3 formation. For this estimate, we include similar reaction patterns in the aqueous phase for
4 MACR as for MVK (Section 3).

5 **2 Experiment-model comparisons**

6 **2.1 Chemical mechanism development**

7 **2.1.1 Kinetic data for individual processes**

8 The analysis of the resulting oligomers was performed by ultra-high-performance liquid
9 chromatography mass spectrometry (UPLC-ESI-MS). All analytical methods are discussed in
10 detail in *Part I*. In brief, the temporal evolution of the MVK, H₂O₂ and O₂ aqueous
11 concentrations and pH were recorded during the laboratory experiments using liquid
12 chromatography UV-DAD absorbance spectroscopy (UPLC-UV, for MVK and H₂O₂
13 concentrations). Dissolved oxygen concentrations and pH were recorded by a multi-parameter
14 analyzer (Consort C3020). The OH concentration in the aqueous phase could not be directly
15 measured. However, it could be derived based on the observed photolytic loss of hydrogen
16 peroxide. Experiments in the absence of MVK revealed a photolysis rate of $9.5(\pm 1.4) \cdot 10^{-6} \text{ s}^{-1}$.
17 This rate decreased as a function of MVK concentrations (Section 2.2.2). Cross-reactions of OH,
18 HO_x and H₂O₂ were included in the model to account for the recycling of these species (HO_x
19 reactions in **Table 1**). The chemical mechanism of MVK decay and oligomer formation as
20 suggested by *Renard et al.* (2013) has been adapted here with some minor modifications in order
21 to constrain kinetic data (**Figure 1**). Not all intermediates were detected during the experiments;
22 however, the structure of the resulting oligomers was used to deduce the most likely reaction
23 pathways. As an α,β -unsaturated carbonyl, MVK bears highly reactive conjugated carbon-
24 carbon and carbon-oxygen double bonds. Therefore, its oxidation by OH might occur via three
25 reaction channels: OH might add to the vinyl group of the MVK molecule either (1) on the β -
26 carbon atom or (2) on the α -carbon atom, or (3) it might abstract a hydrogen atom from either
27 the vinyl group or from the saturated end of the molecule. Pathways (1) and (2) lead to isomeric
28 hydroxyalkyl radicals with identical molecular weights and, thus, neither the initiator radicals nor
29 the resulting oligomers, respectively, are distinguishable with the analytical techniques (mass

1 spectrometry) applied here. In a thorough study of reaction products, Schöne et al. (2014) have
2 identified oxidation products formed on both reaction pathways, but no branching ratio could be
3 determined either.

4 Theoretically, OH addition on the α -carbon atom (pathway 1) is favored on both steric and
5 resonance grounds; the propagating radical formed by this pathway (1) is the more stable one
6 (Odian, 2004; Schöne et al., 2014). An attempt to distinguish between the three pathways was
7 performed by direct observation and quantification of the resulting alkyl radicals using
8 continuous-flow electron paramagnetic resonance (EPR) experiments with MVK concentrations
9 from 1 to 25 mM (Section 1 in the Supplemental Information). The obtained highly complex
10 spectra were the result of superimposition of various EPR signals. Using spectral simulations, the
11 signal of the $\text{HO-CH}_2\text{-}\dot{\text{C}}\text{H-C(O)CH}_3$ radical adduct resulting from pathway (1) was clearly
12 distinguished (dots in **Figure SI**). The proportions of another transient radical was found to
13 depend on the initial MVK concentration (compare the spectra in **Figures S1a and S1b** in the
14 Supplemental Information). A very similar behavior of concentration-dependence of radical
15 species was previously observed in experiments performed on acrylic acid by Gilbert et al.
16 (1994), and they attributed this behavior to the formation of dimer radicals. Therefore, the
17 concentration-dependent radical was attributed to a dimer radical such as $\text{HO-CH}_2\text{-}$
18 $\text{CH(C(O)CH}_3\text{)-CH}_2\text{-}\dot{\text{C}}\text{H-C(O)CH}_3$, thus confirming a very fast recombination pathway (Gilbert
19 et al., 1994). More than two different radical species were present in our experiments, but their
20 respective signals remained unidentified due to overlapping EPR signals in the spectra. Although
21 it was not possible to identify these other radical species, the occurrence of radicals resulting
22 from pathways (2) and (3) was expected, and the EPR experiments showed that their relative
23 importance was much lower than that of pathway (1). In the model, we lump pathways (1) and
24 (2) to the more likely radical from pathway (1) ($k_{\text{MVKOH(a)}}$, **Figure 1**). H-abstraction (pathway 3)
25 might occur most likely on the most weakly bonded H-atoms, which are the ones in the methyl
26 group (bond energy $\sim 94 \text{ kcal mol}^{-1}$, as opposed to $\sim 111 \text{ kcal mol}^{-1}$ for the other H-atoms of the
27 molecule (Blanksby and Ellison, 2002)) and stabilization of the resulting radical due to the
28 adjacent carbonyl group.

29 The overall rate constant for the reaction of MVK with OH has been recently determined as
30 $k_{\text{MVKOH}} = 7.3 \cdot 10^9 \text{ M}^{-1} \text{ s}^{-1}$ (Schöne et al., 2014). Since the branching ratios for the various reaction
31 pathways are not known, we assume that pathway (3) might occur with a similar rate constant as

1 H-abstraction from the structurally-similar acetone ($k_{OH,Acetone} = 1.2 \cdot 10^8 \text{ M}^{-1} \text{ s}^{-1}$ (Ervens et al.,
2 2003; Monod et al., 2005)). The ratio between the overall rate constants $k_{OH,Acetone}/k_{MVKOH} \sim 1.6\%$
3 is in qualitatively good agreement with (i) our EPR results and (ii) the calculation of the possible
4 amounts of H-abstraction reaction by Schöne et al. (2014) that both suggest a minor contribution
5 of the H-abstraction pathway.

6 The resulting alkyl radicals can react with dissolved oxygen to form peroxy radicals RO_2 .
7 The rate constant for this step for all radicals is assumed to be nearly diffusion controlled with
8 $k_{O_2} = 3.1 \cdot 10^9 \text{ M}^{-1} \text{ s}^{-1}$ based on the overview by Neta et al. (1990). In previous model efforts to fit
9 experiments of small organic compounds in aqueous solution, it was assumed that k_{O_2} could be
10 substantially smaller ($k_{O_2} \sim 10^6 \text{ M}^{-1} \text{ s}^{-1}$) (Guzman et al., 2006; Lim et al., 2010; Lim et al., 2013).
11 However, a literature review of rate constants for numerous similar compounds (Alfassi, 1997;
12 Schaefer et al., 2015) reveals that all constants for such reactions are in a range of $2 \cdot 10^9 \text{ M}^{-1} \text{ s}^{-1} <$
13 $k_{O_2} < 4 \cdot 10^9 \text{ M}^{-1} \text{ s}^{-1}$. Only for non-carbon-centered radicals (such as nitrogen-centered radicals),
14 significantly smaller rate constants are observed ($\sim 10^7 - 10^8 \text{ M}^{-1} \text{ s}^{-1}$), and none of them is as low as
15 $k_{O_2} \sim 10^6 \text{ M}^{-1} \text{ s}^{-1}$. An explanation for this discrepancy is the continuous depletion of oxygen
16 during the reactant consumption (Section 2.2.3) that leads to a decrease of the reaction rate (i.e.,
17 the product of rate constant and concentration) with time. Thus, we suggest that in the previous
18 experimental studies, the solutions were temporarily depleted in dissolved oxygen and the
19 reactions occurred with rate constants similar to k_{O_2} as used in the current study. In addition to
20 the reaction with oxygen, the alkyl radicals can react with MVK (k_{olig}) by opening its double
21 bond and forming larger species (oligomer radicals). This process leads to large radicals that
22 contain multiple MVK units and can recombine to form non-radical molecules of oligomers
23 (Section 2.1.2).

24 At various places in the mechanism, rearrangement and recombination reactions of radicals
25 are inferred (k_{arr} and k_{recomb} , respectively). To our knowledge, there is no available literature
26 value for the exact same molecules as inferred in our mechanism. However, several studies
27 suggest rates of the rearrangement reactions (k_{arr}) on the order of $10^6 - 10^7 \text{ s}^{-1}$ (Gilbert et al.,
28 1976; Schuchmann and von Sonntag, 1981, 1984). While no data are available for the ratio
29 k_{arr}/k_{recomb} for the molecules as in our mechanism, we assumed the ratio to be the same as for
30 primary ethers (von Sonntag and Schuchmann, 1997). Since data for the exact compounds are
31 not available, they have been estimated based on those for structurally- similar compounds

1 (NDRL/NIST, 2002). These steps are assumed based on the carbon structure of the resulting
2 detected oligomers. We performed sensitivity studies on the most uncertain and least constrained
3 rate constants. Results are summarized in Section S4 of the supplemental information. They
4 show that the simulation results are insensitive to the choice of k_{arr} and k_{recomb} ; even a change of
5 \pm five orders of magnitude for each of the constants gives the same results as the base case (black
6 line in Figure S3; results of the sensitivity studies are not displayed but would be on top of the
7 base case results) with less than 1% difference. Simultaneous changes of k_{O_2} , k^{1st} or k_{olig} can
8 reproduce similar results for selected experimental conditions; however, the most robust results
9 for all concentration ranges and experimental conditions were obtained for the set of rate
10 constants as summarized in **Table 1**. While this agreement does not necessarily prove that indeed
11 these are the exact rate constants, they reveal important sensitivities and suggest which rate
12 constants should warrant future laboratory experiments.

13 Due to the lack of detailed data on the photolysis of organic hydroperoxides, all photolysis
14 processes of such compounds were assumed to occur with the same rate as H₂O₂ photolysis
15 (Section 2.2.2). This assumption is supported by the similar aqueous phase photolysis rate
16 constants of CH₃OOH, C₂H₅OOH and H₂O₂ (Monod et al., 2000; 2007).

17 **2.1.2 Model treatment of oligomer series**

18 The evolution of the oligomer mass exhibits a three-step kinetics that is characterized by
19 different slopes, i.e., an initial slow increase, when oligomerization is not very efficient yet, a
20 fast increase and a later decrease (cf Figures 3 and 6 in *Part I*). The observed oligomer increase
21 and decrease, together with the determined mass yield, were used to constrain the rate constants
22 in the chemical mechanism for oligomer formation and loss (k_{olig} , k_{loss} in **Figure 1**, respectively).
23 Renard et al. (2013) identified thirteen oligomer series, among which seven series differed in
24 their initiator radical. Each oligomer series showed the typical 'haystack' pattern in the mass
25 spectrum where signals differed by $\Delta m/z$ 70.0419 (corresponding to the exact molecular mass of
26 MVK). The addition of similar unsaturated compounds to initiator radicals usually occurs with
27 rate constants in the range of $10^2 \text{ M}^{-1} \text{ s}^{-1} < k_{olig} < 10^4 \text{ M}^{-1} \text{ s}^{-1}$ (Odian, 2004). However, even
28 applying the upper limit of this range did not lead to sufficiently fast MVK decay and oligomer
29 increase as compared to the observed behavior. Only a value of $k_{olig} = 5 \cdot 10^7 \text{ M}^{-1} \text{ s}^{-1}$ gave a
30 reasonable match between observed and modeled data. The reasons for this discrepancy to
31 literature values are not clear; they might include the facts that (i) no specific kinetic data for
32 MVK oligomerization are available, and this compound, as part of the family of α,β -unsaturated

1 carbonyls, may have a higher oligomerization kinetics than other species, as suggested by
2 *Gilbert et al.* (1994) and by our EPR studies (*Section S1* in the Supplemental Information)
3 and/or (ii) not all MVK-consuming processes are included in the mechanism in *Figure 1*. Such
4 potentially missing pathways will also lead to oligomers, since the predicted oligomer total mass
5 yield from the developed chemical mechanism is similar to the observed one. For all series, we
6 consider the formation of oligomers with up to ten MVK molecules, in agreement with the
7 experimental data that showed most oligomer series had a maximum degree of polymerization
8 ($n = 10$ (with an average $n = 5$)).

9 In the termination step of the radical reaction chain (k^{1st}), the oligomer radicals recombine
10 and disproportionate to form one saturated and one unsaturated product, i.e., yielding compound
11 pairs with $\Delta m/z = 2.0157$. In our chemical mechanism, these oligomer pairs are lumped into one
12 species per series (Oligomers I, III-VII, *Figure 1*). Only Oligomer II is explicitly represented,
13 since it is the only one that originates from peroxy radicals, resulting in a hydroperoxide. It does
14 not form by recombination reaction with itself, but by reaction with the more abundant HO₂
15 radical. The equivalent peroxide compounds from the other series were not detected and are,
16 therefore, not depicted in *Figure 1*. The intermediate radicals are treated explicitly in the
17 mechanism, i.e., 70 different radicals from seven initiator radicals for series I-VII with n MVK
18 molecules ($1 \leq n \leq 10$)), whereas the resulting oligomers are lumped into one single compound
19 per series. For simplicity, we parameterized the termination step by a process of first-order
20 kinetics (k^{1st}). In the literature, second-order rate constants of termination reactions in radical
21 oligomerization are typically in the range of $10^7 - 10^9 \text{ M}^{-1} \text{ s}^{-1}$ (Long et al., 2001). Since these are
22 second-order rate constants, this range is not directly comparable to the fitted value of $k^{1st} =$
23 $6 \cdot 10^4 \text{ s}^{-1}$, but implies that the total radical concentrations might be on the order of $\sim 10^{-5} - 10^{-3} \text{ M}$,
24 which might seem high even in the relatively highly concentrated solutions used here. It should
25 be noted that depending on chain length and/or initiator radical the rate constants for the
26 termination steps might differ. Our mechanism is somewhat simplified, since it is assumed that
27 recombination reactions only occur between molecules of the same series. In reality, these
28 recombination reactions can occur between all radicals. However, since the number of processes
29 in our model would become untraceable for recombination between all 70 radicals (~ 5000
30 possible processes), we chose to only include recombination reactions within the same series. If
31 all possible recombination reactions were taken into account, k^{1st} might be smaller since the same
32 reaction rate could be predicted by assuming a higher radical concentration. In order to keep the
33 number of reactions reasonable within the mechanism, but yet to empirically reproduce the

1 increase in oligomer mass as observed in the experiments by *Renard et al.* (2015), and due to the
2 lack of detailed theoretical or experimental data we assumed the same k^{1st} constants for all
3 oligomer series.

4 The experiments showed that the oligomers continue to react and decrease (Figures 7, 8 and
5 9 in *Part I*). It is assumed that this loss is caused by the continuous oxidation of oligomers by OH
6 or by direct photolysis to smaller, more volatile products. For simplicity, we describe this loss in
7 the model exclusively by the OH radical, even though direct photolysis of carbonyl compounds
8 might be at least as efficient as OH reaction as a loss process (Epstein et al., 2013; Reed-Harris et
9 al., 2014). The fitted OH rate constant ($k_{loss} = 10^8 \text{ M}^{-1} \text{ s}^{-1}$) is on the same order of magnitude as
10 for other large carbonyl compounds (Doussin and Monod (2013))

11 **2.2 Experiment-model comparison: 0.2 mM [MVK]₀ 20 mM**

12 **2.2.1 Input data to the box model**

13 Four laboratory experiments were carried out that differed in the initial MVK concentration
14 ([MVK]₀ = 0.2 mM, 2 mM, 5 mM, and 20 mM, respectively). The ratio of initial MVK and H₂O₂
15 was constant in all experiments ([MVK]₀ / [H₂O₂]₀ = 0.05), in order to favor the reaction of OH
16 with MVK over its reaction with H₂O₂ by more than 90%. Each experiment started with H₂O₂
17 photolysis alone for ~10 min, and then MVK was injected in the solution. Due to the H₂O₂
18 photolysis and other HO_x reactions (*Table 1*), dissolved O₂ concentrations increased during the
19 first 10 minutes, and this increase was faster with higher initial H₂O₂ concentrations. As a
20 consequence, the initial concentration of dissolved oxygen was different for the various initial
21 H₂O₂ concentrations ([O₂]₀ = 284 μM, 358 μM, 436 μM and 505 μM for the four initial MVK
22 concentrations). An additional experiment with [MVK]₀ = 20 mM was also performed in a
23 nearly deoxygenated bulk aqueous phase where [O₂]₀ ~ 60 μM. The concentration of dissolved
24 oxygen was highly variable with time and was continuously measured over the course of the
25 experiments. The solutions were continuously stirred during the experiments. In order to
26 constrain the oxygen concentration in the model, the measured oxygen concentrations for all
27 experiments were fitted and the derived numerical approximations (Section S2 in the
28 Supplemental Information) were used as input data to the box model since mixing (stirring)
29 effects between gas and aqueous phases cannot be reproduced within our simple model
30 framework. The observed increase in dissolved oxygen towards the end of the experiments
31 (*Figures S2b-e*) can be explained by oxygen formation in the recombination reactions of

1 HO₂/O₂⁻ with HO₂ and OH radicals, once MVK is completely consumed (HO_x reactions in **Table**
2 **I**). While this reaction always occurs over the course of the experiments, towards the end of the
3 experiments, insufficient organic compounds are available to form alkyl radicals that could
4 efficiently consume oxygen via peroxy radical formation.

5 A decrease in pH was observed from pH ~ 6 to ~3 for experiments with [MVK]₀ = 2 mM
6 and to pH ~ 4 for [MVK]₀ = 0.2 mM. This evolution was approximated by linear fits as input to
7 the box model (Section 3 in the Supplemental Information). This decrease in pH is likely caused
8 by the formation of organic acids, such as acetic and pyruvic acids (**Figure 1**) and possibly other
9 compounds with acid functionalities that are formed upon oligomer decay (*k_{loss}*) as shown in *Part*
10 *I*. These products are not further tracked in the mechanism.

11 **2.2.2 H₂O₂ photolysis rates as a function of [MVK]₀**

12 The initial decay of MVK is only determined by its reactions with the OH radical (*k_{MVKOH(a)}*
13 and *k_{MVKOH(b)}*, **Figure 1** and **Table 1**). Once a sufficiently high concentration of organic alkyl
14 radicals is present, when most of the dissolved O₂ is consumed, efficient oligomerization starts,
15 which leads to additional loss of MVK. This transition from MVK consumption by only OH to
16 that due to oligomerization can be seen by the two different slopes, denoted by the small blue
17 arrows in **Figure 2b**, where it is most pronounced as compared to less clear features at lower
18 [MVK]₀. Since the initial MVK concentration and *k_{MVKOH}* are known, the only unknown value in
19 determining the initial MVK loss rate is the OH radical concentration in the aqueous phase,
20 which cannot be directly measured. In independent experiments, in the absence of MVK, the loss
21 of H₂O₂ in the aqueous phase was measured (*j_{H2O2}*). The photolysis rate was independent of the
22 initial H₂O₂ concentration (0.4 M and 1 M) and was determined as *j_{H2O2}* = 9.5(±1.4)·10⁻⁶ s⁻¹ in
23 pure water. However, using this value to simulate the initial decay of MVK led to a significant
24 overestimate of this reaction rate, i.e., to a too efficient consumption of MVK, with the largest
25 bias for experiments with the highest [MVK]₀. This finding suggests that the amount of MVK in
26 the solution affects the H₂O₂ photolysis rate due to its light absorbance around 300 nm. Control
27 experiments showed that MVK loss by direct photolysis was negligible compared to oxidation
28 by OH under our experimental conditions (Renard et al., 2013).

29 Measured light intensities were used to calculate the photolysis rate at each MVK
30 concentration according to

1

2

$$J_{H_2O_2} = \int I_{0,\lambda} \times \varepsilon_{\lambda} \times \phi_{\lambda} \times d\lambda \quad (\text{Eq.-1})$$

3

4 where ε_{λ} is H_2O_2 extinction coefficient ($\text{cm}^3 \text{ molec}^{-1} \text{ cm}^{-1}$): it was determined experimentally at
 5 the nm resolution over 236-347 nm, in agreement with previous work (e.g., Kwon and Kwon
 6 (2010)); ϕ_{λ} is the H_2O_2 quantum yield for $\cdot\text{OH}$ production (Herrmann et al., 2010). $I_{0,\lambda}$ is the
 7 spectral irradiance ($\text{photons cm}^{-2} \text{ s}^{-1} \text{ nm}^{-1}$), measured every 1.4 nm (from 241 to 1039 nm) using
 8 a laboratory spectroradiometer (modified SR-500 from Spectral evolution). The resulting
 9 photodissociation coefficient $j_{H_2O_2} = 5.1 (\pm 2.0) \cdot 10^{-6} \text{ s}^{-1}$ obtained by this actinometry calculation
 10 is comparable to the experimentally derived value $9.5 (\pm 1.4) \cdot 10^{-6} \text{ s}^{-1}$. The slightly lower value
 11 obtained by the actinometry calculation may be due to multiple light reflections in the vessel,
 12 that have not been taken into account in the calculation. However, this comparison is done for
 13 the direct photolysis of H_2O_2 alone in pure water.

14 As $j_{H_2O_2}$ is proportional to the incident light intensity, it is likely that its values were sensitive
 15 to the amount of absorbed light by MVK, depending on its concentration. Knowing the
 16 absorbance spectrum of MVK (experimentally determined $A_{MVK,\lambda}$), one can calculate the
 17 resulting irradiance spectrum $I'_{0,\lambda}$ theoretically available for H_2O_2 photolysis (eq. 2).

18

19

$$I'_{0,\lambda} = I_{0,\lambda} \times 10^{-A_{MVK,\lambda}} \quad (\text{Eq.-2})$$

20

21 Using this new irradiance spectrum, one can calculate the corresponding photodissociation
 22 coefficient $j'_{H_2O_2}$ (s^{-1}) (equation 3).

23

24

$$j'_{H_2O_2} = \int I'_{0,\lambda} \times \varepsilon_{\lambda} \times \phi_{\lambda} \times d\lambda \quad (\text{Eq.-3})$$

25

26 Using the experimentally determined values of $A_{MVK,\lambda}$ at different MVK concentrations, the
 27 resulting values of $j'_{H_2O_2}$ are compared (**Figure 3**) to the experimental values, where the kinetics
 28 of H_2O_2 decomposition have been monitored during MVK reactivity initiated at different MVK
 29 concentrations. The results show the same decreasing trend of $j_{H_2O_2}$ with increasing MVK
 30 concentrations for both experimentally and actinometry-derived data. The actinometry

1 calculations give slightly smaller values, but this can be explained by possible multiple light
2 reflections in the vessel that have not been taken into account in the calculation.

3 In addition to these theoretical and experimental data, **Figure 3** includes photolysis rates as
4 used in the model calculations that were adjusted to match the initial MVK loss in the
5 experiments. This loss is solely ascribed to the reaction of MVK with OH, and the only fitting
6 parameter in this reaction rate is the OH concentration that depends directly on $j_{H_2O_2}$. It should be
7 noted that the actinometry-derived data are based on the assumption of a constant (initial) MVK
8 concentration while the model and experimental data take into account decreasing MVK
9 concentrations. For example, at the highest initial MVK concentration (20 mM) where MVK
10 complete decay takes more than 100 min, model, experimental and actinometry-derived data are
11 in good agreement. Globally, one would expect the model to agree with the experimental data
12 rather than with the actinometry ones, which is the case for low and high initial concentrations of
13 MVK, but it is not clear why the model better matches actinometry data at intermediate MVK
14 concentrations.

15 **2.2.3 Predicted MVK decay**

16 Comparison of the MVK decay to the evolution of dissolved oxygen (**Figures 2 S2** in the
17 Supplemental Information) shows that MVK consumption accelerates when oxygen is (mostly)
18 consumed. Under such conditions, the reactions of organic radicals with oxygen (k_{O_2} in **Figure**
19 **1**) become negligible, and oligomerization under nearly anaerobic conditions takes place. At low
20 $[MVK]_0$ (0.2 mM), the MVK consumption occurs over much shorter time scales than at higher
21 initial concentrations, and the competition between OH reaction and oligomerization is not
22 clearly seen. **Figure 2e** shows MVK decay for $[MVK]_0 = 20$ mM under initially low O_2
23 conditions, for which the reaction solution was saturated with argon. In comparison to **Figure**
24 **2a**, it is obvious that the initial slow MVK decay is missing, and MVK is quickly consumed as of
25 the beginning of the experiment. Note the different time scales in the figures that clearly show
26 that the reaction is completed within about half of the time at low oxygen concentrations. This
27 sensitivity to oxygen concentrations is in agreement with the general faster oligomerization rate
28 under low oxygen conditions that is well known from polymer chemistry (Odian, 2004; Mendez
29 et al., 2013). While the reaction cell represents an aqueous volume with a very small
30 surface/volume ratio, it will be explored in Section 3.2.2 if such oxygen limitation occurs in
31 atmospheric multiphase systems.

1 In theory, it might be possible that MVK and its oxidation products might be also consumed
2 by reaction with H₂O₂. In order to estimate this loss, control experiments were conducted to
3 check for any reactivity of H₂O₂ towards MVK. MVK (20 mM) and H₂O₂ (400 mM) were mixed
4 for 300 min in the dark. No significant consumption of MVK or formation of oligomers was
5 detected. Among the intermediate reaction products formed, the only reactive species towards
6 H₂O₂ are pyruvic acid, glycolaldehyde and glyoxal (2-4%, 11% and 4% molar yield,
7 respectively, from MVK in the aqueous phase (Zhang et al., 2010; Schöne et al., 2014). Under
8 our experimental conditions, the rate constants of these species with H₂O₂ (Schöne and
9 Herrmann, 2014) suggest life times of $\tau \sim 22$ s for pyruvic acid, $\tau \sim 62$ s for glycolaldehyde and
10 $\tau > 4$ h for glyoxal. While the latter is greater than our experimental time scales, the two former
11 ones are certainly occurring in the vessel during our experiments. The reaction of pyruvic acid
12 with H₂O₂ leads to the production of acetic acid with molar yield (Stefan and Bolton, 1999;
13 Schöne et al., 2014)). Because acetic acid is one of the identified oligomer contributor (Oligomer
14 series IV), the reaction of pyruvic acid with H₂O₂ might, thus, artificially increase the amount of
15 oligomers formed. Taking into account the molar yields of acetic acid (57%) and pyruvic acid (2-
16 4%) (Zhang et al. 2010; Schöne et al 2014), one can conclude that this increase in oligomers is
17 negligible. The reaction of glycolaldehyde with H₂O₂ leads to the production of formic acid with
18 molar yield (Schöne and Herrmann, 2014; Stefan and Bolton, 1999). However, formic acid was
19 not identified as a precursor of oligomers in our experiments; therefore, the reaction of
20 glycolaldehyde with H₂O₂ is not assumed to influence the amount of SOA detected.

21 **2.2.4 Predicted oligomer formation and decay**

22 *Figure 4* shows a qualitative comparison of predicted and observed temporal evolution of
23 the total oligomers for the five cases depicted in *Figure 2*. The observed total oligomer mass and
24 yield were determined by means of scanning mobility particle sizer (SMPS) measurements of the
25 nebulized solutions (cf. *Part I*). In the model, the oligomer mass represents a net yield, since it is
26 the steady-state concentration from simultaneous oligomer formation (k^{1st}) and loss (k_{loss})
27 (*Figure 1*). Despite different units, we compare the temporal evolution and the relative
28 differences for the predicted oligomer concentrations for the four initial concentrations (and low
29 oxygen for [MVK]₀ = 20 mM) (*Figure 4a*). Assuming an average molecular weight for all
30 oligomers (mass for initiator radical + $n \cdot$ MVK units ($n = 5$)) the two units can be linearly
31 converted; however, for model purposes, we show all model results in M. The predicted
32 differences of oligomer concentrations between [MVK]₀ = 20 mM and [MVK]₀ = 2 mM are 1-2

1 orders of magnitude, in agreement with the experiments. At even lower $[\text{MVK}]_0 = 0.2 \text{ mM}$,
2 oligomer formation becomes very inefficient. Reasons of this non-linearity between initial MVK
3 concentrations and oligomer mass might include the formation of small, volatile compounds,
4 such as (di)acids, that are not explicitly treated by the model. Both experimental and model data
5 show that at the highest $[\text{MVK}]_0$, oligomer mass keeps increasing beyond the experimental time
6 scale ($t = 90 \text{ min}$), whereas it is decaying for the lower $[\text{MVK}]_0$. This behavior is in agreement
7 with the results shown in **Figure 2**, where it is shown that for the lower initial concentrations,
8 MVK is essentially consumed at that time, and no further oligomers can be formed and the loss
9 reaction dominates. While it has been discussed in *Part I* that oligomer formation is
10 characterized by an initially slow increase in mass, followed by a fast increase and then a
11 decrease, the first step is somewhat obscured in **Figure 4** due to the logarithmic scale. Model
12 results for $[\text{MVK}]_0 = 20 \text{ mM}$ for high and low dissolved oxygen, respectively, shows initially a
13 much higher oligomerization rate for the latter case, in agreement with the more efficient and
14 faster MVK decay in **Figure 2e** as compared to **Figure 2a**. Comparison of the oligomer increase
15 to experimental data for the 'low oxygen case' is not performed, since it was not recorded during
16 the experiments.

17 The predicted evolution of individual oligomer series is shown in **Figure 5** for $[\text{MVK}]_0 = 20$
18 mM under conditions of high and low initial oxygen concentration. At high initial oxygen
19 concentration, Oligomer II (**Figure 1**) is the main contributor to the total oligomer concentration.
20 This oligomer series is the only one that is directly formed from a peroxy radical whereas all
21 others are formed from alkyl radicals and thus are suppressed as long as dissolved oxygen is
22 available. As expected, under low oxygen conditions, the concentration of Oligomer II is (much)
23 smaller and Oligomer I has the highest concentration. Despite the lower oxygen concentration,
24 the resulting concentration of Oligomer II is decreased by about an order of magnitude, but it
25 still has the second highest concentration, followed by Oligomers III and VII. These oligomers
26 need the fewest reaction steps and, thus, form most efficiently as opposed to those at the bottom
27 of **Figure 1** (Oligomers IV, V, and VI). UPLC-ESI mass spectra of the product distribution upon
28 MVK oxidation and oligomerization showed that the concentration maximum of the individual
29 series occurred at $\sim 90 \text{ min}$ of photooxidation. At that reaction time, assuming the oligomer
30 relative concentrations were proportional to the relative mass spectra peak intensities, the
31 concentrations of all detected oligomer series were in a range of two orders of magnitude
32 (Renard et al., 2013); in the mass spectra data treatment, any series that contributed $< 1\%$ as the
33 most intense peak was ignored. This result is not quite in agreement with the model results

1 shown in *Figure 5*, where the spread between the different oligomer concentrations spans about
2 four orders of magnitude. This discrepancy might be due to our simplified assumptions that all
3 oligomerization steps occur with the same rate constant, independently of their initiator radical
4 and of their chain length. Odian (2004) showed that (i) oligomerization slows down with
5 increasing degree of polymerization (n) and (ii) the initial oligomerization rates for small n might
6 be different for different initiator radicals. Due to the lack of any detailed information on these
7 explicit steps and trends for the individual oligomer series in our mechanism, we did not perform
8 any further refinement of the rate constants. Instead in the following section, we limit our
9 discussion to the prediction of total oligomers, i.e., the sum of Oligomers I - VII since the total
10 mass yield (nearly 100%) is in reasonable agreement with experiments. Note that for the estimate
11 of the mass yield as predicted by the model, we assumed a constant molecular weight based on
12 oligomers of five monomer units. While this estimate seems a reasonable average as the
13 abundance of larger oligomers decreased with chain length, the variation of the chain length over
14 time leads to changes in molecular weight and therefore in mass yield. The maximum mass yield
15 in the experiments was 59% ($[MVK]_0 = 20$ mM) and therefore differs by less than a factor of two
16 from that as predicted by the model.

17 **3 Multiphase simulations**

18 **3.1 Phase partitioning of organics into aerosol water**

19 **3.1.1 Setchenov coefficients**

20 Henry's law constants are defined for the partitioning of species between the gas and pure
21 aqueous phases. Several model and observational studies have shown that for many inorganic
22 and organic compounds Henry's law constants can be used to describe the partitioning into cloud
23 and fog water, resulting in reasonable agreement with measurements (Ervens, 2015). However,
24 due to much higher salt concentrations in aerosol water, this aqueous medium does not comprise
25 an ideal solution and therefore Henry's law constants should not be applied. The Setchenov
26 coefficient K_s [kg mol^{-1}] represents a proportionality factor for the ratio of solubilities in pure
27 water (K_H) and in salt solutions (K_H^*) (Wang et al., 2014; Sander, 2015). This ratio depends on
28 the molality of the salt solution [mol kg^{-1}].
29

$$30 \quad \log \left(\frac{K_H}{K_H^*} \right) = K_s [\text{salt}] \quad (\text{Eq.-4})$$

1
2 Positive K_s values point to a salting-out effect, i.e. to reduced solubility in salt solutions as
3 compared to pure water, whereas negative values point to a salting-in effect. The comprehensive
4 study by Wang et al. (2014) shows that Setchenov coefficients for ketones in ammonium sulfate
5 solutions are in the range of $\sim 0.4 < K_s [\text{kg mol}^{-1}] < 0.6$ and in NaCl solutions $0.18 < K_s [\text{kg mol}^{-1}] < 0.33$, and therefore ketones undergo a salting-out effect in these solutions. Opposite trends
6 were found for glyoxal ($K_s = -0.24(\pm 0.02) \text{ kg mol}^{-1}$) in ammonium sulfate solutions (Kampf et
7 al., 2013). To the best of our knowledge, measurements of the Setchenov coefficient for methyl
8 vinyl ketone or methacrolein (MACR) in salt solutions are not available. Therefore in the
9 following, we apply a maximum value enhancement of $K_H^*/K_H = 100$ which seems applicable
10 for a saturated ammonium sulfate solution and a Setchenov coefficient of $K_S \sim 0.5 \text{ kg mol}^{-1}$
11 (**Figure 6**). In general, the Setchenov coefficients depend on the nature of the dissolved salt
12 (e.g., univalent, bivalent) and other parameters such as temperature. In the case of oxygen, it has
13 been shown that both organic (Lang, 1996) and inorganic (Battino et al., 1983) salts have a
14 similar impact on oxygen solubility and both lead to a weak salting-out effect.
15

16 **3.1.2 Solubility and abundance of oligomer precursors**

17 **Figure 6** suggests that the solubility of ketones might be reduced by a factor of ~ 100 in
18 saturated ammonium sulfate solutions as are encountered at relative humidities $\sim 80\%$. The
19 resulting value $K_H^* = 0.41 \text{ M atm}^{-1}$, using the value determined in pure water $K_{H,MVK} = 41 \text{ M}$
20 atm^{-1} (Iraci et al., 1999) is much smaller than the value as determined in concentrated sulfuric
21 acid solutions (80%) ($K_{H,MVK} = 3000 \text{ M atm}^{-1}$ (Noziere et al., 2006)). On the other hand, MVK
22 and its oligomers might accumulate near the air/water interface of aerosols as observed for other
23 compounds (Donaldson and Valsaraj, 2010) which would lead to a MVK concentration in the
24 condensed phase in excess to that predicted based on K_H . Such separation from the bulk aqueous
25 phase would favor heterogeneous reactions occurring at the interface, where organic
26 concentrations are enhanced as compared to the bulk.

27 MVK can be considered a proxy compound for similar unsaturated organics that might
28 undergo similar reactions. Therefore, the concentration of potential oligomer precursors is likely
29 greater in aerosol water than the dissolved fraction of a single compound might suggest. Lim et
30 al. (2010) stated that millimolar aqueous concentrations (c_{aq}) can be considered reasonable level
31 of aqSOA precursors in aerosol water (liquid water content, LWC). This concentration
32 corresponds to a mass concentration of a few ng m^{-3} :

$$LWC \left(\frac{20 \cdot 10^{-6} \text{ g}_{\text{H}_2\text{O}}}{\text{m}_3^3} \right) \cdot c_{aq} \left(\frac{10^{-3} \text{ mol}_{org}}{\text{L}_{\text{H}_2\text{O}}} \right) \cdot M_{org} \left(\frac{150 \text{ g}_{org}}{\text{mol}_{org}} \right) \cdot \frac{\text{L}_{\text{H}_2\text{O}}}{1000 \text{ g}_{\text{H}_2\text{O}}} = 3 \text{ ng m}^{-3} \quad (\text{Eq.-5})$$

for an average molecular weight of $M_{org} = 150 \text{ g mol}^{-1}$ for organics and a water density of 1 kg L^{-1} . Ambient mass concentrations of several 10's, up to 100's ng m^{-3} were determined for small carbonyl compounds in the particulate phase (Kawamura et al., 2013). The comparison of these ranges to the estimate in Eq.-5 shows that (i) the concentration of organics in aerosol water might be much higher than millimolar, and/or (ii) only a small fraction of particulate organics is required to initiate significant oligomer formation as observed in the laboratory experiments. Therefore, we also explore in the following model studies the efficiency of oligomerization using $K_H^*(\text{MVK})$ and a case where the aqueous phase concentration of unsaturated compounds, with MVK being a proxy, is on the order of $\sim 10^{-3} - 1 \text{ M}$ as an upper limit of the total of potential oligomer precursors.

One other oligomer precursor is MACR, which is the other main first-generation oxidation product from isoprene. MVK and MACR are formed with gas phase yields of 29% and 21% (with some variations, depending on NO_x levels), respectively (Galloway et al., 2011). Bulk aqueous phase experiments have shown that also MACR efficiently forms oligomers in the aqueous phase (ElHaddad et al., 2009; Liu et al., 2009; Michaud et al., 2009), but mechanistic information as detailed as for MVK is not available. MACR is less soluble than MVK ($K_{H,MACR} = 6.5 \text{ M atm}^{-1}$), but it has a slightly higher rate constant with OH in the aqueous phase, $k_{MACROH} = 9.4 \cdot 10^9 \text{ M}^{-1} \text{ s}^{-1}$ (Schöne et al., 2014). The mass yields of oligomers from MACR are similar to those as observed for MVK; however, the diversity of detected oligomer series is higher (Liu et al., 2012). Instead of developing an explicit chemical mechanism for MACR, in the following, we estimate its potential SOA formation efficiency scaled by that of MVK, given that both its OH reactivity and its overall oligomerization potential are known.

While the initial MACR decay might be somewhat faster than that for MVK, we assume that the kinetics of the subsequent MACR decay due to oligomerization and oligomer formation is comparable to that of MVK. Overall, the oligomer formation might then be approximated by a single reaction:



1 In order to estimate the rate constant for (R-3), k_{R-3} , we seek a rate constant that represents
2 best the oligomer formation as predicted by the explicit mechanism in *Figure 1*. In *Figure S4*,
3 (Supplemental Information), the black line shows simulations for several cases that only include
4 MVK for various conditions. The other lines show model results for which the reactions
5 involving MVK (i.e., initial OH reaction and the subsequent oligomerization steps) were
6 replaced by R-3 with different k_{R-3} values. While it is obvious that such a single reaction step
7 cannot fully reproduce the wide range of oligomerization rates as predicted by the explicit
8 mechanism, k_{R-3} can be bounded by $1 \cdot 10^9 \text{ M}^{-1} \text{ s}^{-1} < k_{R-3} < 1.5 \cdot 10^9 \text{ M}^{-1} \text{ s}^{-1}$ as it reproduces for most
9 cases both the temporal evolution and the final oligomer mass reasonably well. In the following
10 model studies, we use therefore an average value of $k_{R-3} = 1.5 \cdot 10^9 \text{ M}^{-1} \text{ s}^{-1}$ in order to describe the
11 OH-initiated oligomerization from MACR, whereas we apply the full mechanism (*Figure 1* and
12 *Table 1*) for MVK. We do not suggest that oligomerization by any of these compounds should be
13 indeed represented by R-3 in future model studies, since both the temporal evolution and the
14 kinetics might be different for other conditions (N_a , LWC, $[\text{OH}_{(aq)}]$, [WSOC] etc). The only
15 purpose of k_{R-3} is to develop a shortcut that allows us to estimate the role of oligomerization from
16 MACR in our model and to roughly estimate and compare its aqSOA formation potential.

17 **3.2 Description of the box model and initial conditions**

18 In order to assess the importance of oligomerization as an aqSOA source under atmospheric
19 conditions, we apply the same box model as in Section 2. However, instead of initializing
20 aqSOA precursors, O_2 and H_2O_2 in the aqueous phase, gas phase species are initialized, and their
21 uptake into the aqueous phase of aerosol particles is described by the resistance model
22 (Schwartz, 1986). Initial gas phase mixing ratios and uptake parameters are summarized in *Table*
23 *2*. In the atmospheric multiphase system, MVK is also oxidized in the gas phase by OH; other
24 sinks that are likely less important (direct photolysis, reaction with O_3) are not considered here. It
25 is assumed that both H_2O_2 and O_2 have constant gas phase mixing ratios over the course of the
26 simulations (1 ppb and 0.21 atm, respectively). It is assumed that all organic products (oligomers
27 and smaller oxidation products, Figure 1) remain in the aqueous phase. This simplification might
28 bias the predicted oligomer formation rates since small products such as acetic or pyruvic acids
29 might evaporate due to their low vapor pressure. However, in the atmosphere, these compounds
30 might be produced by other processes in the gas phase and be taken up into the aqueous phase
31 and initiate oligomer formation via the processes described here. Since our model studies are

1 considered being very exploratory at this point, we assume that our assumption of no evaporation
2 might affect the predicted oligomer masses only to a minor extent.

3 The aqueous phase is composed of aqueous particles with a diameter of $D_{wet} = 200$ nm and a
4 concentration $N_a = 5000$ cm⁻³, which gives a total liquid water content of LWC ~ 20 $\mu\text{g m}^{-3}$,
5 being typical for deliquesced aerosol particle loadings in the atmosphere.

6

7 **3.3 Model results**

8 **3.3.1 Comparison to gasSOA formation**

9 In the gas phase, only MACR forms SOA whereas MVK does not show any (detectable)
10 SOA formation (Kroll et al., 2006; Surratt et al., 2006). SOA yields from isoprene are in the
11 range of ~ 0 -5%, depending on oxidant, RH and NO_x levels (Carlton et al., 2009), and irradiation
12 sources employed (Carter et al., 1995; Brégonzio-Rozier et al., 2015). In order to explore the
13 simultaneous SOA formation from isoprene in the gas and aqueous phases, we simulate the
14 multiphase system as shown in *Figure 7*. The kinetic data for gas phase reactions and uptake
15 processes are summarized in *Tables 2 and 3*. For simplicity, the SOA yield from MACR is
16 adjusted such that the overall gasSOA yield is $\sim 2\%$ (= 21% yield of MACR from isoprene
17 multiplied by 10% SOA yield from MACR, resulting in a value (2.1%) that is in the range of
18 observed SOA yields from isoprene). The other products (volatile organic compounds, VOCs)
19 are not further tracked in the model, since they do not contribute to SOA mass. AqSOA
20 formation from MVK occurs via the mechanism displayed in *Figure 1* and *Table 1*; aqSOA
21 formation from MACR is approximated by k_{R-3} . The model is initialized with 2 ppb isoprene and
22 $5 \cdot 10^6$ cm⁻³ OH in the gas phase, both of which are kept constant; initial values for MVK and
23 MACR are set to zero.

24 Simulations are performed for model cases over six hours. Results are shown in *Figure 8*
25 after two and six hours of simulation time, respectively. GasSOA masses are not affected by
26 different loss rates into the aqueous phase. Unlike in chamber experiments, we assume a constant
27 mixing ratio of isoprene (2 ppb) throughout the simulation. Therefore, the total SOA mass cannot
28 be directly related to this initial mixing ratio in order to calculate a SOA yield as done in
29 laboratory experiments. The ratio of resulting SOA mass to initial isoprene (2 ppb ~ 5560 ng m⁻³
30 ³) is $\sim 3\%$ for gasSOA after 6 h (180 ng m⁻³ / 5560 ng m⁻³) whereas it is in a range of < 0.01 -

1 20% for aqSOA. The temporal evolution of the predicted SOA (oligomer) masses is different in
2 the laboratory experiments and the multiphase model since in the former oligomer formation
3 rates are very high in the beginning but slow down when MVK is consumed. In the latter, the
4 constant isoprene and oxidant concentrations in the gas phase provide an infinite supply of
5 oligomer precursors (MVK, MACR), O₂ and OH and therefore their ratios do not change over
6 the simulation time.

7 Based on several bulk aqueous laboratory experiments (*Part I*), aqSOA yields of ~60% have
8 been reported for oligomerization from MVK. The multiphase model simulations as performed
9 here show that such values should be discussed with caution in the context of atmospheric
10 implications. Only if simultaneous gas phase losses and uptake rates into the aqueous phase are
11 taken into account, a solid comparison of aqSOA and gasSOA yields is feasible. Our simulations
12 show that – even if 100% of dissolved aqSOA precursors (MVK, MACR) is converted into
13 oligomers, the overall aqSOA yield in the multiphase system might be significantly smaller (<<
14 1%).

15 **3.3.2 Base case: $K_H^* = 0.01 \cdot K_H$**

16 As discussed in Section 3.2.2, the solubility of MVK and MACR might be reduced in
17 aerosol water by a factor up to 100 as compared to solubility in pure water. Under those
18 conditions, the resulting aqueous concentrations of MACR and MVK using the multiphase
19 scheme in *Figure 7* are much smaller than the lowest ones (0.2 mM) as used in the laboratory
20 experiments discussed in *Section 2*. As can be seen in *Figure 4*, the amount of oligomers is not
21 proportionally related to the initial concentration, but it is lower by several orders of magnitude
22 as that predicted for a 10 times higher initial MVK concentration. Note that an important
23 difference between the multiphase simulations and the simulations mimicking the laboratory
24 experiments in *Section 2* are the temporal differences in the absolute MVK concentrations and
25 concentration ratios (e.g., [MVK]/[OH]_{aq}). While in the laboratory experiments MVK is
26 completely consumed within 30 - 100 minutes (*Figure 2*), in the atmospheric multiphase system
27 the assumption of a constant supply seems reasonable (over relatively short time scales as
28 simulated here) since constant isoprene emissions will provide always sufficient MVK and
29 MACR. These differences cause a different temporal evolution of predicted oligomer masses.
30 The results in *Figure 8* show that for the reduced solubility of MVK and MACR as it likely

1 exists in aerosol water, the contribution of oligomers to total predicted SOA is negligible ($\ll 1$
2 ng m^{-3} after 6 h). While not shown, it can be expected that even partitioning of MVK and MACR
3 according to their Henry's law constants (K_H) might not be sufficient to initiate efficient oligomer
4 formation in the aqueous phase.

5 **3.3.3 Total initial oligomer precursor concentration**

6 As suggested by Eq-5 and the fact that not only MVK and MACR but also structurally
7 similar compounds might undergo oligomerization, we performed some sensitivity studies with
8 different initial potential oligomer precursor concentrations. If a few ng m^{-3} of these precursors,
9 resulting in a total aqueous concentration of ~ 20 mM, are dissolved in aerosol water, the
10 predicted oligomer mass is still $< 1\%$ of predicted gasSOA mass at all times (**Figure 8**). Only if a
11 substantial fraction of all dissolved water-soluble organic carbon might act as oligomer precursor
12 ($[\text{Org}]_{\text{aq}} = 1$ M, ~ 150 ng m^{-3} according to Eq.-5), oligomers might substantially add to the total
13 SOA mass. This estimate should likely be considered an upper limit. However, to date, only a
14 small fraction of the total organic carbon fraction of aerosols can be usually identified on a
15 molecular level (Herckes et al., 2013); therefore, an exact estimate of the fraction of oligomer
16 precursors in organic aerosols cannot be given.

17 Unlike in laboratory experiments, atmospheric aqueous aerosol particles can be considered
18 saturated with oxygen (~ 270 μM) due to their large surface-volume-ratio. In all our model
19 sensitivity studies, the oxygen concentration reached saturation level after a few seconds. Even
20 this initial period seems an artifact and likely does not occur in the atmosphere where particles
21 are continuously exposed to ambient air. Therefore, in the atmosphere, oligomerization occurs on
22 longer time scales as in the laboratory where oxygen might be consumed over relatively short
23 time scales (**Figure S2**). Under atmospheric conditions, radical oligomerization (k_{olig}) competes
24 with the fast O_2 addition on primary initiating and propagating radicals. The latter yields peroxy
25 radicals (RO_2^\bullet), which are moderately reactive and can terminate propagation or may even
26 initiate slow reactions of polymerization (Odian, 2004; Ligon et al., 2014).

27 **3.3.4 Oxygen solubility**

28 Similar to most organics, oxygen exhibits a salting-out effect, i.e., $K_H(\text{O}_2)/K_H^*(\text{O}_2)$ is
29 greater than unity (Eq.-5). Depending on the salt and ionic strength, the solubility of oxygen in

1 aerosol water might be reduced by up to an order of magnitude (Battino et al., 1983; Lang,
2 1996). While under such conditions oxygen still reaches its equilibrium concentration, the molar
3 ratio of oligomer precursors to dissolved oxygen approaches a value, above which efficient
4 oligomerization in the atmosphere has been predicted ($[\text{oligomer precursors}] / [\text{O}_2] \sim 50$) (Renard
5 et al., 2013).

6 Under such conditions, oligomer formation in aerosol water might substantially increase as
7 compared to higher dissolved oxygen concentrations (cf third and last bars in *Figure 8*). It
8 should be noted that these simulations are very exploratory, and the concentration of dissolved
9 oxygen in atmospheric waters has not been measured to date yet. The strong decrease in oxygen
10 solubility, as we imply here, might only occur in very concentrated aerosol water. Under such
11 conditions, chemical reactions might also be affected by ionic strength effects and therefore rate
12 constants as listed in *Table 1* might differ. However, it seems obvious that also other
13 combinations of $[\text{Org}]_{\text{aq}}$ and $K_H^*(\text{O}_2)$ might lead to similar results as shown in the last bars in
14 *Figure 8*. Therefore, we conclude that under specific conditions in the atmosphere radical
15 oligomerization in aerosol water might contribute a non-negligible fraction to the total SOA
16 loading, in addition to other pathways, such as gasSOA formation or other pathways in the
17 condensed phase.

18

19 **4 Summary and conclusions**

20 We have derived a comprehensive chemical mechanism of the oligomerization of methyl
21 vinyl ketone (MVK) in the aqueous phase, based on bulk aqueous phase laboratory studies that
22 are described in previous work (Renard et al., 2013, 2015 (*Part I*)). Using this mechanism, model
23 studies mimic the observed decay of MVK for a wide range of initial concentrations (0.2 mM
24 $[\text{MVK}(\text{aq})]_0 \sim 20$ mM). The different oligomerization rates for high and low aqueous phase
25 concentrations of oxygen, respectively, can be reproduced by the model. This sensitivity occurs
26 because alkyl radicals that are formed by OH oxidation of MVK can react either with oxygen
27 forming peroxy radicals or with another MVK molecule, which leads to oligomers. Sensitivity
28 studies of individual rate constants show that the derived mechanism is robust over a wide range
29 of experimental conditions, and the set of rate constants is consistent with literature values for
30 similar compounds.

1 The chemical mechanism is implemented into a multiphase box model that is initialized with
2 isoprene (2 ppb) and OH in the gas phase. MVK, together with methacrolein (MACR) represent
3 the main oxidation products of isoprene in the atmosphere. Even small SOA yields from isoprene
4 oxidation products in the gas phase have been considered to contribute substantially to the total
5 global SOA burden due to the high emission rate of isoprene. In an exploratory study, we
6 compared the potential additional contributions of MVK and MACR oligomerization in the
7 aerosol aqueous phase to the total predicted SOA mass. Our model results show that,
8 oligomerization by MVK and MACR in aerosol particles is likely not efficient under
9 atmospheric conditions, in particular since the partitioning of MVK and MACR is reduced due to
10 salting-out effects. MVK and MACR can be considered as two precursors of likely many more
11 structurally similar compounds in the atmosphere. If a small fraction of organic aerosol carbon
12 ($\sim 100 \text{ ng m}^{-3}$) is comprised of such compounds, resulting in aqueous phase concentrations of ~ 1
13 M, their oligomerization might contribute a few percent to total predicted SOA mass.

14 While in laboratory experiments solutions often are not saturated with oxygen, such
15 conditions are likely not met in the atmosphere due to the large surface-to-volume ratio of
16 ambient aerosol particles (and cloud droplets) that allows an efficient replenishment of consumed
17 oxygen. However, while organics might exhibit salting-in or salting-out effects in salt solutions,
18 oxygen are always salted-out, i.e., it is less soluble in aerosol water than in pure water. If the
19 oxygen solubility is reduced by one order of magnitude (as observed in concentrated salt
20 solutions), a small fraction of total organic carbon ($\sim \text{few ng m}^{-3}$) is sufficient to act as efficient
21 oligomer precursors. In summary, our study can be regarded as an initial step towards a better
22 understanding of oligomerization reactions and their potential role as SOA source in the
23 atmosphere. Our model results suggest that under specific conditions the oligomerization of the
24 total of unsaturated organics in aerosol water might contribute up to $\sim 20\%$ to total predicted
25 SOA in the atmosphere.

26 **Acknowledgement**

27 All authors are thankful to Veronica Vaida and Barney Ellison for valuable discussions on the
28 chemical mechanism. B.E. acknowledges support from NOAA's climate goal. A.M.
29 acknowledges support from CIRES (visiting fellowship) and the National Research Agency
30 ANR (project CUMULUS ANR-2010-BLAN-617-01), P.R. acknowledges AXA insurances for

1 funding this research.

2 **References**

- 3 Alfassi, Z. B.: The chemistry of free radicals: Peroxyl radicals, 1st ed., Wiley, West Sussex,
4 England, 1997.
- 5 Altieri, K., Carlton, A. G., Lim, H., Turpin, B. J., and Seitzinger, S. P.: Evidence for oligomer
6 formation in clouds: Reaction of isoprene oxidation products, *Environ. Sci. Technol.*, 40,
7 16,4956-4960, 2006.
- 8 Altieri, K. E., Turpin, B. J., and Seitzinger, S. P.: Oligomers, organosulfates, and nitrooxy
9 organosulfates in rain water identified by ultra-high resolution electrospray ionization FT-ICR
10 mass spectrometry, *Atmos. Chem. Phys.*, 9,2533-2542, 2009.
- 11 Arakaki, T., Anastasio, C., Kuroki, Y., Nakajima, H., Okada, K., Kotani, Y., Handa, D., Azechi,
12 S., Kimura, T., Tshako, A., and Miyagi, Y.: A general scavenging rate constant for reaction
13 of hydroxyl radical with organic carbon in atmospheric waters, *Environ. Sci. Technol.*, 47,
14 15,8196–8203, 10.1021/es401927b, 2013.
- 15 Atkinson, R.: Kinetics and mechanisms of the gas-phase reactions of the hydroxyl radical with
16 organic compounds under atmospheric conditions, *Chem. Rev.*, 86, 1,69-201,
17 10.1021/cr00071a004, 1986.
- 18 Baboukas, E. D., Kanakidou, M., and Mihalopoulos, N.: Carboxylic acids in gas and particulate
19 phase above the Atlantic Ocean, *J. Geophys. Res. - Atmos.*, 105, D11,14459-14471, 2000.
- 20 Battino, R., Rettich, T. R., and Tominaga, T.: The solubility of oxygen and ozone in liquids, *J.*
21 *Phys. Chem. Ref. Data* 12, 2,163-178, 1983.
- 22 Bielski, B. H. J., Cabell, D. E., Arudi, R. L., and Ross, A. B.: Reactivity of HO₂/O₂⁻ radicals in
23 aqueous solution, *J. Phys. Chem. Ref. Data*, 14, 4,1041-1100, 1985.
- 24 Blanksby, S. J., and Ellison, G. B.: Bond dissociation energies of organic molecules, *Acc. Chem.*
25 *Res.*, 2002.
- 26 Brégonzio-Rozier, L., Siekmann, F., Giorio, C., Pangui, E., Morales, S. B., Temime-Roussel, B.,
27 Gratien, A., Michoud, V., Ravier, S., Cazaunau, M., Tapparo, A., Monod, A., and Doussin, J.
28 F.: Gaseous products and secondary organic aerosol formation during long term oxidation of
29 isoprene and methacrolein, *Atmos. Chem. Phys.*, 15, 6,2953-2968, 10.5194/acp-15-2953-
30 2015, 2015.

1 Carlton, A. G., Wiedinmyer, C., and Kroll, J. H.: A review of Secondary Organic Aerosol (SOA)
2 formation from isoprene, *Atmos. Chem. Phys.*, 9, 14,4987-5005, 10.5194/acp-9-4987-2009,
3 2009.

4 Carter, W. P. L., Luo, D., Malkina, I. L., and Pierce, J. A.: Environmental chamber studies of
5 atmospheric reactivities of volatile organic compounds. Effects of varying chamber and light
6 source, California Air Resources Board Contract A032-0692, and South Coast Air Quality
7 Management District Coordinating Research Council, Inc., Project M-9, 1995.

8 Chin, M., and Wine, P. H.: A temperature-dependent competitive kinetics study of the aqueous-
9 phase reactions of OH radicals with formate, formic acid, acetate, acetic acid and hydrated
10 formaldehyde, in: *Aquatic and Surface Photochemistry*, edited by: G. R. Helz, Zepp, R. G.,
11 and Crosby, D. G., Lewis Publishers, Boca Raton, 85 - 96, 1994.

12 Christensen, H., Sehested, K., and Corfitzen, H.: Reactions of hydroxyl radicals with hydrogen
13 peroxide at ambient and elevated temperatures, *J. Phys. Chem.*, 86, 9,1588-1590,
14 10.1021/j100206a023, 1982.

15 Denkenberger, K. A., Moffet, R. C., Holecek, J. C., Robetier, T. P., and Prather, K. A.: Real-
16 time, single-particle measurements of oligomers in aged ambient aerosol particles, *Environ.*
17 *Sci. Technol.*, 41, 15,5439-5446, 2007.

18 Donahue, N. M., Epstein, S. A., Pandis, S. N., and Robinson, A. L.: A two-dimensional volatility
19 basis set: 1. organic-aerosol mixing thermodynamics, *Atmos. Chem. Phys.*, 11, 7,3303-3318,
20 10.5194/acp-11-3303-2011, 2011.

21 Donahue, N. M., Robinson, A. L., Stanier, C. O., and Pandis, S. N.: Coupled partitioning,
22 dilution and chemical aging of semivolatile organics, *Environ. Sci. Technol.*, 40,2635-2643,
23 2006.

24 Donaldson, D. J., and Valsaraj, K. T.: Adsorption and reaction of trace gas-phase organic
25 compounds on atmospheric water film surfaces: A critical review, *Environ. Sci. Technol.*, 44,
26 3,865-873, 10.1021/es902720s, 2010.

27 Doussin, J. F., and Monod, A.: Structure–activity relationship for the estimation of OH-oxidation
28 rate constants of carbonyl compounds in the aqueous phase, *Atmos. Chem. Phys.*, 13,
29 23,11625-11641, 10.5194/acp-13-11625-2013, 2013.

30 ElHaddad, I., Liu, Y., Scarfoglio, M., Nieto-Gligorovski, L., Michaud, V., Temime-Roussel,

1 B., Quivet, E., Marchand, N., Sellegri, K., and Monod, A.: In-cloud processes of methacrolein
2 under simulated conditions - Part 2: Formation of Secondary Organic Aerosol, *Atmos. Chem.*
3 *Phys.*, 9,5107-5117, 2009.

4 Elliot, A. J., and Buxton, G. V.: Temperature dependence of the reactions $\text{OH} + \text{O}_2^-$ and $\text{OH} +$
5 HO_2 in water up to 200°C, *J. Chem. Soc. Faraday Trans.*, 88,2465-2470, 1992.

6 Epstein, S. A., Tapavicza, E., Furche, F., and Nizkorodov, S. A.: Direct photolysis of carbonyl
7 compounds dissolved in cloud and fog~droplets, *Atmos. Chem. Phys.*, 13, 18,9461-9477,
8 10.5194/acp-13-9461-2013, 2013.

9 Ervens, B.: Modeling the Processing of Aerosol and Trace Gases in Clouds and Fogs, *Chemical*
10 *Reviews*, 10.1021/cr5005887, 2015.

11 Ervens, B., Gligorovski, S., and Herrmann, H.: Temperature dependent rate constants for
12 hydroxyl radical reactions with organic compounds in aqueous solution, *Phys. Chem. Chem.*
13 *Phys.*, 5,1811-1824, 2003.

14 Ervens, B., Turpin, B. J., and Weber, R. J.: Secondary organic aerosol formation in cloud
15 droplets and aqueous particles (aqSOA): a review of laboratory, field and model studies,
16 *Atmos. Chem. Phys.*, 11, 21,11069–11102, doi:10.5194/acp-11-11069-2011, 2011.

17 Galloway, M. M., Huisman, A. J., Yee, L. D., Chan, A. W. H., Loza, C. L., Seinfeld, J. H., and
18 Keutsch, F. N.: Yields of oxidized volatile organic compounds during the OH radical initiated
19 oxidation of isoprene, methyl vinyl ketone, and methacrolein under high-NO_x conditions,
20 *Atmos. Chem. Phys.*, 11, 21,10779-10790, 10.5194/acp-11-10779-2011, 2011.

21 Gilbert, B. C., Holmes, R. G. G., Laue, H. A. H., and Norman, R. O. C.: Electron spin resonance
22 studies. Part L. Reactions of alkoxy radicals generated from alkyl hydroperoxides and
23 titanium(III) ion in aqueous solution, *Journal of the Chemical Society, Perkin Transactions 2*,
24 9,1047-1052, 10.1039/p29760001047, 1976.

25 Gilbert, B. C., Smith, J. R. L., Milne, E. C., Whitwood, A. C., and Taylor, P.: Kinetic and
26 structural EPR studies of radical polymerization. Monomer, dimer, trimer and mid-chain
27 radicals formed via the initiation of polymerization of acrylic acid and related compounds
28 with electrophilic radicals ([radical dot]OH, SO₄-[radical dot] and Cl₂-[radical dot]), *J.*
29 *Chem. Soc., Perkin Transactions 2*, 8,1759-1769, 10.1039/p29940001759, 1994.

30 Guzman, M. I., Colussi, A. J., and Hoffmann, M. R.: Photoinduced oligomerization of aqueous

1 pyruvic acid, *J. Phys. Chem. A*, 110, 10,3619–3626, 2006.

2 Hanson, D. R., Burkholder, J. B., Howard, C. J., and Ravishankara, A. R.: Measurement of
3 hydroxyl and hydroperoxy radical uptake coefficients on water and sulfuric acid surfaces, *J.*
4 *Phys. Chem.* , 96, 12,4979-4985, 10.1021/j100191a046, 1992.

5 Healy, R. M., Wenger, J. C., Metzger, A., Duplissy, J., Kalberer, M., and Dommen, J.:
6 Gas/particle partitioning of carbonyls in the photooxidation of isoprene and 1,3,5-trimethyl
7 benzene, *Atmos. Chem. Phys.*, 8,3215-3230, 2008.

8 Herckes, P., Valsaraj, K. T., and Collett Jr, J. L.: A review of observations of organic matter in
9 fogs and clouds: Origin, processing and fate, *Atmos. Res.*, 132–133, 0,434-449,
10 <http://dx.doi.org/10.1016/j.atmosres.2013.06.005>, 2013.

11 Herrmann, H., Hoffmann, D., Schaefer, T., Brüner, P., and Tilgner, A.: Tropospheric Aqueous-
12 Phase Free-Radical Chemistry: Radical Sources, Spectra, Reaction Kinetics and Prediction
13 Tools, *ChemPhysChem*, 11, 18,3796-3822, 10.1002/cphc.201000533, 2010.

14 Iraci, L. T., Baker, B. M., Tyndall, G. S., and Orlando, J. J.: Measurements of the Henry's law
15 coefficients of 2-methyl-3-buten-2-ol, methacrolein, and methylvinyl ketone, *J. Atmos.*
16 *Chem.*, 33,321-330, 1999.

17 Kalberer, M., D. Paulsen, M. Sax, M. Steinbacher, J. Dommen, A. S. H. Prevot, R. Fisseha, E.
18 Weingartner, V. Frankevich, R. Zenobi, and Baltensperger, U.: Identification of polymers as
19 major components of atmospheric organic aerosols, *Science*, 303,1659-1662, 2004.

20 Kampf, C. J., Waxman, E. M., Slowik, J. G., Dommen, J., Pfaffenberger, L., Praplan, A. P.,
21 Prévôt, A. S. H., Baltensperger, U., Hoffmann, T., and Volkamer, R.: Effective Henry's Law
22 Partitioning and the Salting Constant of Glyoxal in Aerosols Containing Sulfate,
23 *Environmental Science & Technology*, 10.1021/es400083d, 2013.

24 Kanakidou, M., J. H. Seinfeld, S. Pandis, I. Barnes, F. J. Dentener, M. C. Facchini, R. van
25 Dingenen, B. Ervens, A. Nenes, C. J. Nielsen, E. Swietlicki, J.P. Putaud, Y. Balkanski, C. E.,
26 S. F., J. Hjorth, G. Moortgat, R. Winterhalter, C. E. L. Myhre, K. Tsigaridis, E. Vignati, E.
27 Stephanou, and Wilson, J.: Organic aerosol and global climate modelling: A review, *Atmos.*
28 *Chem. Phys.*, 5,1-70, 2005.

29 Kawamura, K., Okuzawa, K., Aggarwal, S. G., Irie, H., Kanaya, Y., and Wang, Z.:
30 Determination of gaseous and particulate carbonyls (glycolaldehyde, hydroxyacetone,

1 glyoxal, methylglyoxal, nonanal and decanal) in the atmosphere at Mt. Tai, Atmos. Chem.
2 Phys., 13, 10,5369-5380, 10.5194/acp-13-5369-2013, 2013.

3 Kroll, J. H., Ng, N. L., Murphy, S. M., Flagan, R. C., and Seinfeld, J. H.: Secondary organic
4 aerosol formation from isoprene photooxidation under high NO_x conditions, Geophys. Res.
5 Lett., 32, L18808,doi: 10.1029/2005GL023637, 2005.

6 Kroll, J. H., Ng, N. L., Murphy, S. M., Flagan, R. C., and Seinfeld, J. H.: Secondary organic
7 aerosol formation from isoprene photooxidation, Environ. Sci. Technol., 40, 6,1869-1877,
8 2006.

9 Kuwata, M., Liu, Y., McKinney, K., and Martin, S. T.: Physical state and acidity of inorganic
10 sulfate can regulate the production of secondary organic material from isoprene
11 photooxidation products, Physical Chemistry Chemical Physics, 17, 8,5670-5678,
12 10.1039/c4cp04942j, 2015.

13 Kwon, B. G., and Kwon, J.-H.: Measurement of the hydroxyl radical formation from H₂O₂,
14 NO₃⁻, and Fe(III) using a continuous flow injection analysis, Journal of Industrial and
15 Engineering Chemistry, 16, 2,193-199, <http://dx.doi.org/10.1016/j.jiec.2009.10.007>, 2010.

16 Lang, W.: Setchenov coefficients for oxygen in aqueous solutions of various organic
17 compounds, Fluid Phase Equilibria, 114, 1–2,123-133, [http://dx.doi.org/10.1016/0378-](http://dx.doi.org/10.1016/0378-3812(95)02823-4)
18 [3812\(95\)02823-4](http://dx.doi.org/10.1016/0378-3812(95)02823-4), 1996.

19 Ligon, S. C., Husár, B., Wutzel, H., Holman, R., and Liska, R.: Strategies to Reduce Oxygen
20 Inhibition in Photoinduced Polymerization, Chemical Reviews, 114, 1,557-589,
21 10.1021/cr3005197, 2014.

22 Lim, Y. B., Tan, Y., Perri, M. J., Seitzinger, S. P., and Turpin, B. J.: Aqueous chemistry and its
23 role in secondary organic aerosol (SOA) formation, Atmos. Chem. Phys., 10, 21,10521-
24 10539, 2010.

25 Lim, Y. B., Tan, Y., and Turpin, B. J.: Chemical insights, explicit chemistry, and yields of
26 secondary organic aerosol from OH radical oxidation of methylglyoxal and glyoxal in the
27 aqueous phase, Atmos. Chem. Phys., 13, 17,8651-8667, 10.5194/acp-13-8651-2013, 2013.

28 Lind, J. A., and Kok, G. L.: Henry's law Determinations for aqueous solutions of hydrogen
29 peroxide, methylhydroperoxide and peroxyacetic acid J. Geophys. Res. , 91, D7,7889-7895,
30 1986.

1 Liu, Y., ElHaddad, I., Scarfogliero, M., Nieto-Gligorovski, L., Temime-Roussel, B., Quivet, E.,
2 Marchand, N., Picquet-Varrault, B., and Monod, A.: In-cloud processes of methacrolein under
3 simulated conditions - Part 1: Aqueous phase photooxidation, *Atmos. Chem. Phys.*, 9,5093-
4 5105, 2009.

5 Liu, Y., Monod, A., Tritscher, T., Praplan, A. P., DeCarlo, P. F., Temime-Roussel, B., Quivet,
6 E., Marchand, N., Dommen, J., and Baltensperger, U.: Aqueous phase processing of
7 secondary organic aerosol from isoprene photooxidation, *Atmos. Chem. Phys.*, 12, 13,5879-
8 5895, 10.5194/acp-12-5879-2012, 2012.

9 Long, T. E., McGrath, J. E., and Richard, S.: Polymers, Synthesis, pp. 751-774, in: *Encyclopedia*
10 *of physical science and technology*, Polymers, 3rd ed., edited by: Meyers, R. A., Academic
11 Press, New York, 2001.

12 Mackay, D., and Shiu, W. Y.: A critical review of Henry's law constants for chemicals of
13 environmental interest, *J. Phys. Chem. Ref. Data* 10, 4,1175-1199, 1981.

14 Matsunaga, S. N., Kato, S., Yoshino, A., Greenberg, J. P., Kajii, Y., and Guenther, A. B.: Gas-
15 aerosol partitioning of semi volatile carbonyls in polluted atmosphere in Hachioji, Tokyo,
16 *Geophys. Res. Lett.*, 32, 11,L11805, 10.1029/2004gl021893, 2005.

17 Mazzoleni, L. R., Ehrmann, B. M., Shen, X., Marshall, A. G., and Collett, J. L.: Water-soluble
18 atmospheric organic matter in fog: Exact masses and chemical formula identification by
19 ultrahigh-resolution Fourier transform ion cyclotron resonance mass Spectrometry, *Environ.*
20 *Sci. Technol.*, 44, 10,3690-3697, 10.1021/es903409k, 2010.

21 Mead, R. N., Felix, J. D., Avery, G. B., Kieber, R. J., Willey, J. D., and Podgorski, D. C.:
22 Characterization of CHOS compounds in rainwater from continental and coastal storms by
23 ultrahigh resolution mass spectrometry, *Atmospheric Environment*, 105, 0,162-168,
24 <http://dx.doi.org/10.1016/j.atmosenv.2015.01.057>, 2015.

25 Mead, R. N., Mullaugh, K. M., Brooks Avery, G., Kieber, R. J., Willey, J. D., and Podgorski, D.
26 C.: Insights into dissolved organic matter complexity in rainwater from continental and
27 coastal storms by ultrahigh resolution Fourier transform ion cyclotron resonance mass
28 spectrometry, *Atmos. Chem. Phys.*, 13, 9,4829-4838, 10.5194/acp-13-4829-2013, 2013.

29 Mendez, M., Ciuraru, R., Gosselin, S., Batut, S., Visez, N., and Petitprez, D.: Reactivity of
30 chlorine radical with submicron palmitic acid particles: kinetic measurements and product

1 identification, *Atmos. Chem. Phys.*, 13, 23,11661-11673, 10.5194/acp-13-11661-2013, 2013.

2 Michaud, V., El Haddad, I., Liu, Y., Sellegri, K., Laj, P., Villani, P., Picard, D., Marchand, N.,
3 and Monod, A.: In-cloud processes of methacrolein under simulated conditions – Part 3:
4 Hygroscopic and volatility properties of the formed secondary organic aerosol, *Atmos. Chem.*
5 *Phys.*, 9, 14,5119- 5130, 2009.

6 Monod, A., Chebbi, A., Durand-Jolibois, R., and Carlier, P.: Oxidation of methanol by hydroxyl
7 radicals in aqueous solution under simulated cloud droplet conditions, *Atmos. Environ.*,
8 34,5283-5294, 2000.

9 Monod, A., Chevallier, E., Jolibos, R. D., Doussin, J. F., Picquet-Varrault, B., and Carlier, P.:
10 Photooxidation of methylhydroperoxide and ethylhydroperoxide in the aqueous phase under
11 simulated cloud droplet conditions, *Atmos. Environ.*, 41,2412-2426, 2007.

12 Monod, A., L. Poulain, S. Grubert, Voisin, D., and Wortham, H.: Kinetics of OH-initiated
13 oxidation of oxygenated organic compounds in the aqueous phase: new rate constants,
14 structure-activity relationships and atmospheric implications, *Atmos. Environ.*, 39,7667-7688,
15 2005.

16 NDRL/NIST: Solution Kinetics Database on the Web, in, <http://kinetics.nist.gov/solution/>, 2002.

17 Neta, P., Huie, R. E., and Ross, A. B.: Rate constants for reactions of peroxy radicals in fluid
18 solutions, *J. Phys. Chem. Ref. Data*, 19, 2,413-513, 1990.

19 Nozriere, B., Dziedzic, P., and Cordova, A.: Inorganic ammonium salts and carbonate salts are
20 efficient catalysts for aldol condensation in atmospheric aerosols, *Physical Chemistry*
21 *Chemical Physics*, 12, 15,3864-3872, 2010.

22 Nozriere, B., Voisin, D., Longfellow, C. A., Friedli, H., Henry, B. E., and Hanson, D. R.: The
23 uptake of methyl vinyl ketone, methacrolein, and 2-methyl-3-butene-2-ol onto sulfuric acid
24 solutions, *J. Phys. Chem. A*, 110 7,2387–2395, 2006.

25 Odian, G.: *Principles of Polymerization*, John Wiley & Sons Inc., Hoboken, New Jersey, 835
26 pp., 2004.

27 Odum, J. R., Hoffmann, T., Bowman, F., Collins, D., Flagan, R. C., and Seinfeld, J. H.:
28 Gas/particle partitioning and secondary organic aerosol yields, *Environ. Sci. Technol.*,
29 30,2580-2585, 1996.

30 Paasivirta, J., Sinkkonen, S., Mikkelsen, P., Rantio, T., and Wania, F.: Estimation of Vapor

1 Pressures, Solubilities and Henry's Law Constants of selected persistent organic Pollutants as
2 Functions of Temperature, *Chemosphere*, 39, 5,811-832, 1999.

3 Polidori, A., Turpin, B. J., Davidson, C. I., Rodenburg, L. A., and Maimone, F.: Organic PM_{2.5}:
4 Fractionation by polarity, FTIR Spectroscopy, and OM/OC ratio for the Pittsburgh aerosol,
5 *Aer. Sci. Tech.*, 42, 3,233 - 246, 2008.

6 Reed-Harris, A., B. Ervens, R. K. Shoemaker, E. C. Griffith, R. J. Rapf, J. Kroll, A. Monod, and
7 Vaida, V.: Photochemical kinetics of pyruvic acid in aqueous solution, *J. Phys. Chem. A*, 118,
8 37,8505–8516, 2014.

9 Renard, P., Siekmann, F., Gandolfo, A., Socorro, J., Salque, G., Ravier, S., Quivet, E., Clément,
10 J. L., Traikia, M., Delort, A. M., Voisin, D., Thissen, R., and Monod, A.: Radical mechanisms
11 of methyl vinyl ketone oligomerization through aqueous phase OH-oxidation: on the
12 paradoxical role of dissolved molecular oxygen, *Atmos. Chem. Phys.*, 13,6473-6491,
13 10.5194/acp-13-6473-2013, 2013.

14 Renard, P., Siekmann, F., Salque, G., Smaani, A., Demelas, C., Coulomb, B., Vassalo, L.,
15 Ravier, S., Temime-Roussel, B., Voisin, D., and Monod, A.: Aqueous phase oligomerization
16 of methyl vinyl ketone through photooxidation – Part 1: Aging processes of oligomers,
17 *Atmos. Chem. Phys.*, 15,51-35, 10.5194/acp-15-21-2015, 2015.

18 Sander, R.: Compilation of Henry's law constants (version 4.0) for water as solvent, *Atmos.*
19 *Chem. Phys.*, 15, 8,4399-4981, 10.5194/acp-15-4399-2015, 2015.

20 Schaefer, T., Schindelka, J., Hoffmann, D., and Herrmann, H.: Laboratory kinetic and
21 mechanistic studies on the OH-initiated oxidation of acetone in aqueous solution, *J. Phys.*
22 *Chem. A*, 116, 24,6317-6326, 10.1021/jp2120753, 2012.

23 Schaefer, T., van Pinxteren, D., and Herrmann, H.: Multiphase Chemistry of Glyoxal: Revised
24 Kinetics of the Alkyl Radical Reaction with Molecular Oxygen and the Reaction of Glyoxal
25 with OH, NO₃, and SO₄⁻ in Aqueous Solution, *Environmental Science & Technology*, 49,
26 1,343-350, 10.1021/es505860s, 2015.

27 Schöne, L., Schindelka, J., Szeremeta, E., Schaefer, T., Hoffmann, D., Rudzinski, K. J.,
28 Szmigielski, R., and Herrmann, H.: Atmospheric aqueous phase radical chemistry of the
29 isoprene oxidation products methacrolein, methyl vinyl ketone, methacrylic acid and acrylic
30 acid - kinetics and product studies, *Phys. Chem. Chem. Phys.*, 16,6257-6272

1 10.1039/c3cp54859g, 2014.

2 Schuchmann, H.-P., and von Sonntag, C.: Photolysis at 185 nm of dimethyl ether in aqueous
3 solution: involvement of the hydroxymethyl radical, *Journal of Photochemistry*, 16, 4,289-
4 295, [http://dx.doi.org/10.1016/0047-2670\(81\)80051-2](http://dx.doi.org/10.1016/0047-2670(81)80051-2), 1981.

5 Schuchmann, H.-P., and Von Sonntag, C.: Methylperoxyl Radicals: A Study of the y-
6 Radiolysis of Methane in Oxygenated Aqueous Solutions, *Z. Naturforschung*, 39b,217-221,
7 1984.

8 Schwartz, S.: Mass transport considerations pertinent to aqueous phase reactions of gases in
9 liquid water clouds, in: *Chemistry of Multiphase Atmospheric Systems*, edited by: Jaeschke,
10 W., NATO ASI Series, Springer, Berlin, 415-471, 1986.

11 Stefan, M. I., and Bolton, J. R.: Reinvestigation of the acetone degradation mechanism in dilute
12 aqueous solution by the UV/H₂O₂ process, *Environ. Sci. Technol.*, 33,870-873, 1999.

13 Surratt, J. D., S. M. Murphy, J. H. Kroll, N. L. Ng, L. Hildebrandt, A. Sorooshian, R.
14 Szmigielski, R. Vermeylen, W. Maenhaut, M. Claeys, R. C. Flagan, and Seinfeld, J. H.:
15 Chemical composition of secondary organic aerosol formed from the photooxidation of
16 isoprene, *J. Phys. Chem. A*, 110, 31,9665–9690, doi: 10.1021/jp061734m, 2006.

17 Tolocka, M. P., M. Jang, J. M. Ginter, F. J. Cox, Kamens, R. M., and Johnston, M. J.: Formation
18 of oligomers in secondary organic aerosol, *Environ. Sci. Technol.*, 38, 5,1428-1434, 2004.

19 Trump, E. R., and Donahue, N. M.: Oligomer formation within secondary organic aerosols:
20 equilibrium and dynamic considerations, *Atmos. Chem. Phys.*, 14, 7,3691-3701, 10.5194/acp-
21 14-3691-2014, 2014.

22 von Sonntag, C., and Schuchmann, H.-P.: Peroxyl radicals in aqueous solution, in: *Peroxyl*
23 *Radicals*, edited by: Alfassi, Z. B., Wiley, Chichester, 173–234, 1997.

24 Wang, C., Lei, Y. D., Endo, S., and Wania, F.: Measuring and Modeling the Salting-out Effect in
25 Ammonium Sulfate Solutions, *Environmental Science & Technology*, 48, 22,13238-13245,
26 10.1021/es5035602, 2014.

27 Zhang, H., and Ying, Q.: Secondary organic aerosol formation and source apportionment in
28 Southeast Texas, *Atmos. Environ.*, 45, 19,3217-3227, DOI: 10.1016/j.atmosenv.2011.03.046,
29 2011.

30 Zhang, Q., Jimenez, J. L., Canagaratna, M. R., Allan, J. D., Coe, H., Ulbrich, I., Alfarra, M. R.,

1 Takami, A., Middlebrook, A. M., Sun, Y. L., Dzepina, K., Dunlea, E., Docherty, K., DeCarlo,
2 P. F., Salcedo, D., Onasch, T., Jayne, J. T., Miyoshi, T., Shimo, A., Hatakeyama, S.,
3 Takegawa, N., Kondo, Y., Schneider, J., Drewnick, F., Borrmann, S., Weier, S., Demerjian,
4 K., Williams, P., Bower, K., Bahreini, R., Cottrell, L., Griffin, R. J., Rautiainen, J., Sun, J. Y.,
5 Zhang, Y. M., and Worsnop, D. R.: Ubiquity and dominance of oxygenated species in organic
6 aerosols in anthropogenically-influenced Northern Hemisphere midlatitudes, *Geophys. Res.*
7 *Letts.*, 34, 13, L13801, doi: 10.1029/2007GL029979, 2007.

8 Zhang, X., Chen, Z. M., and Zhao, Y.: Laboratory simulation for the aqueous OH-oxidation of
9 methyl vinyl ketone and methacrolein: significance to the in-cloud SOA production, *Atmos.*
10 *Chem. Phys.*, 10, 19, 9551-9561, 10.5194/acp-10-9551-2010, 2010.

11
12

1 **Table 1.** Rate constants (at 298 K) for the processes in Figure 1.
2

Symbol	Description	k	Reference/Comment
$k_{\text{MVKOH(a)}}$	Oxidation of MVK by OH radical, addition to the C=C bond	$7.18 \cdot 10^9 \text{ M}^{-1} \text{ s}^{-1}$	The total rate constant is $k_{\text{MVKOH}} = 7.3 \cdot 10^9 \text{ M}^{-1} \text{ s}^{-1}$ (Schöne et al., 2014) The branching ratio (98.4% / 1.6%) was set based on EPR studies (cf text and Section S1 in SI)
$k_{\text{MVKOH(b)}}$	Oxidation of MVK by OH radical, H-abstraction from methyl group	$1.17 \cdot 10^8 \text{ M}^{-1} \text{ s}^{-1}$	
k_{O_2}	Peroxy radical formation from alkyl radicals	$3.1 \cdot 10^9 \text{ M}^{-1} \text{ s}^{-1}$	Average value of rate constant $\text{R} \cdot + \text{O}_2$ (Neta et al., 1990)
$k_{\text{olig}}^{*})$	Addition of n^{th} MVK (1 n 10)	$5 \cdot 10^7 \text{ M}^{-1} \text{ s}^{-1}$	$k=10^2\text{-}10^4 \text{ M}^{-1} \text{ s}^{-1}$ in Odian, 2004
$k_{\text{loss}}^{*})$	Oxidation of oligomers by OH radical	$10^8 \text{ M}^{-1} \text{ s}^{-1}$	Average k_{OH} for large organic compounds, e.g., Arakaki et al. (2013)
j_{ROOH}	Photolysis of hydroperoxides	Same as $j_{\text{H}_2\text{O}_2}$	
$k^{1\text{st } *})$	Simplified 1 st order reaction: Conversion of oligomer radicals to stable products	$6 \cdot 10^4 \text{ s}^{-1}$	Estimated in order to reproduce observed increase in oligomer mass (Section 2.2.4)
$k_{\text{arr}}^{*})$	Rearrangement reaction	$8 \cdot 10^6 \text{ s}^{-1}$	(Gilbert et al., 1994)
$k_{\text{recomb}}^{*})$	Recombination of radicals	$2.4 \cdot 10^6 \text{ s}^{-1}$	Estimated as 30% of k_{arr}
k_{MglyOH}	Oxidation of methylglyoxal by OH radical	$6.1 \cdot 10^8 \text{ M}^{-1} \text{ s}^{-1}$	(Schaefer et al., 2012)
k_{HAcOH}	Oxidation of acetic acid/acetate by OH radical	$1.5 \cdot 10^7 \text{ M}^{-1} \text{ s}^{-1}$ (HAc) $10^8 \text{ M}^{-1} \text{ s}^{-1}$ (Ac ⁻)	(Chin and Wine, 1994)
k_{HO_2}	Recombination reaction of RO_2 with HO_2/O_2^-	$8 \cdot 10^5 \text{ M}^{-1} \text{ s}^{-1}$ (HO_2) $9.7 \cdot 10^7 \text{ M}^{-1} \text{ s}^{-1}$ (O_2^-)	Estimated equal to $\text{HO}_2 + \text{HO}_2/\text{O}_2^-$

1 **Table 1, continued**

2

HO_x reactions		
$\text{H}_2\text{O}_2 + \text{h}\nu \rightarrow 2 \text{OH}$	$j_{\text{H}_2\text{O}_2} = f([\text{MVK}]_0)$	Experimentally determined, cf. Figure 3
$\text{H}_2\text{O}_2 + \text{OH} \rightarrow \text{HO}_2 + \text{H}_2\text{O}$	$3 \cdot 10^7 \text{ M}^{-1} \text{ s}^{-1}$	(Christensen et al., 1982)
$\text{HO}_2 + \text{HO}_2/\text{O}_2^- \rightarrow \text{O}_2 + \text{H}_2\text{O}_2$	$8 \cdot 10^5 \text{ M}^{-1} \text{ s}^{-1} (\text{HO}_2)$ $9.7 \cdot 10^7 \text{ M}^{-1} \text{ s}^{-1} (\text{O}_2^-)$	(Bielski et al., 1985)
$\text{OH} + \text{HO}_2/\text{O}_2^- \rightarrow \text{H}_2\text{O} + \text{O}_2$	$10^{10} \text{ M}^{-1} \text{ s}^{-1}$	(Elliot and Buxton, 1992)
WSOC reactions (Section 3.2)		
$\text{WSOC} + \text{OH} \rightarrow \text{R}\cdot + \text{HO}_2$	$3.8 \cdot 10^8 \text{ M}^{-1} \text{ s}^{-1}$	(Arakaki et al., 2013)
$\text{R}\cdot + \text{O}_2 \rightarrow \text{RO}_2$	$3.1 \cdot 10^9 \text{ M}^{-1} \text{ s}^{-1}$	(Neta et al., 1990)

3

4 *) For sensitivity studies on these constants, cf Section S4 in the Supplemental Information.

1 **Table 2.** Uptake parameters and initial conditions for box model multiphase simulations

Uptake parameters	
Mass accommodation coefficient for MVK, MACR, H ₂ O ₂ , OH	$\alpha = 1$
Gas phase diffusion coefficient for MVK, MACR, H ₂ O ₂ , OH	$D_g = 2 \cdot 10^{-5} \text{ cm}^2 \text{ s}^{-1}$
$K_H^*(\text{MVK}) = K_H(\text{MVK}) \cdot 100$ ¹⁾	0.41 - 41 M atm ⁻¹
$K_H^*(\text{MACR}) = K_H(\text{MACR}) \cdot 100$ ¹⁾	6.5 - 650 M atm ⁻¹
$K_H(\text{H}_2\text{O}_2)$ ²⁾	10^5 M atm^{-1}
$K_H(\text{OH})$ ³⁾	30 M atm ⁻¹
$K_H(\text{O}_2)$ ⁴⁾	0.0013 M atm ⁻¹
Constant gas phase mixing ratios or concentrations	
Isoprene	2 ppb
H ₂ O ₂	1 ppb
O ₂	0.21 atm
OH	$5 \cdot 10^6 \text{ cm}^{-3}$
Aerosol parameter	
Particle diameter	$D_{\text{wet}} = 200 \text{ nm}$
Particle concentration	$N_a = 5000 \text{ cm}^{-3}$
Total aerosol liquid water content	$\sim 20 \mu\text{g m}^{-3}$

2
3 ¹⁾ The lower value of this range denotes reduced KH* due to solubility reduction in ionic
4 solutions (**Figure 6**). The upper values are the intrinsic Henry's law constants and were taken
5 from (Iraci et al., 1999); ²⁾(Lind and Kok, 1986) ³⁾ (Hanson et al., 1992); ⁴⁾ (Sander, 2015)

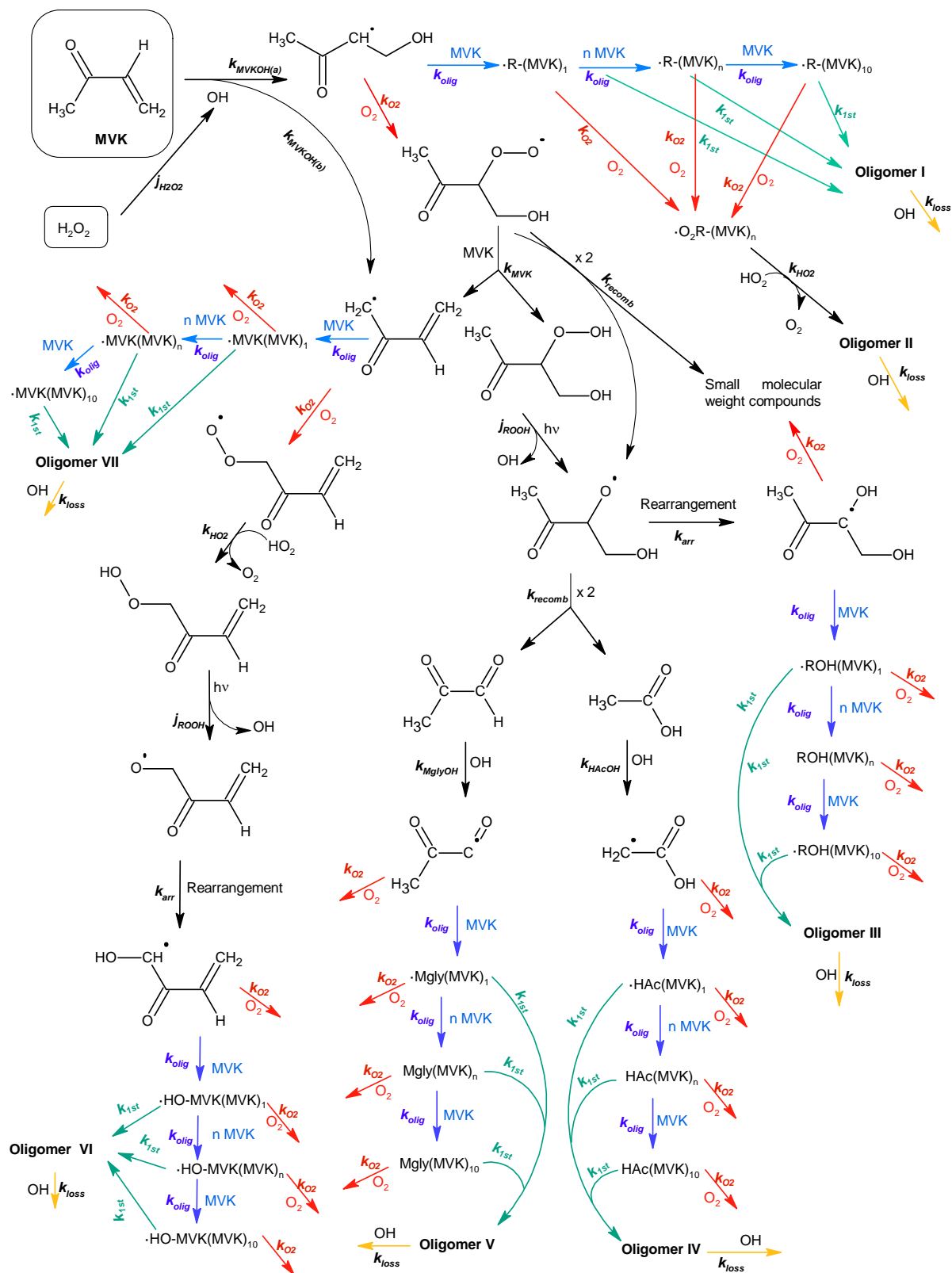
1 **Table 3.** Kinetic parameters for gas phase reactions for the multiphase simulations to compare aqSOA and gasSOA formation from
 2 isoprene (Figure 7)

3

	k (cm ³ s ⁻¹)	Reference
Gas phase reactions		
Isoprene + OH → 0.29 MVK + 0.21 MACR	1 · 10 ⁻¹⁰	(Atkinson, 1986)
MVK + OH → VOC	1.85 · 10 ⁻¹¹	(Atkinson, 1986)
MACR + OH → VOC + 0.1 SOA	3.07 · 10 ⁻¹¹	(Atkinson, 1986)

4

5



1
 2 **Figure 1.** Chemical mechanism, constrained by laboratory studies for different conditions
 3 $[\text{MVK}]_0, [\text{H}_2\text{O}_2]_0$. All rate constants are summarized in Table 1.

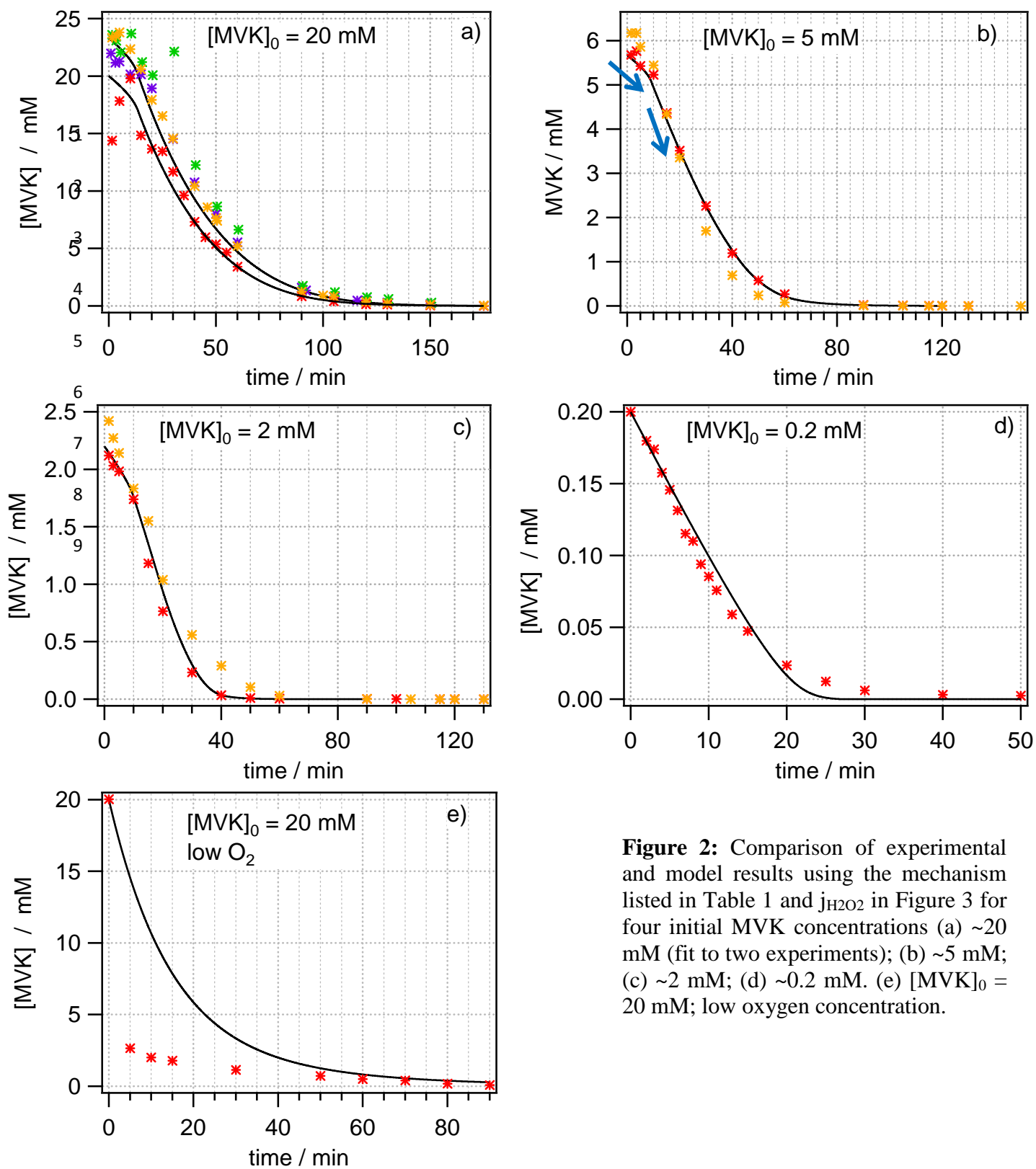
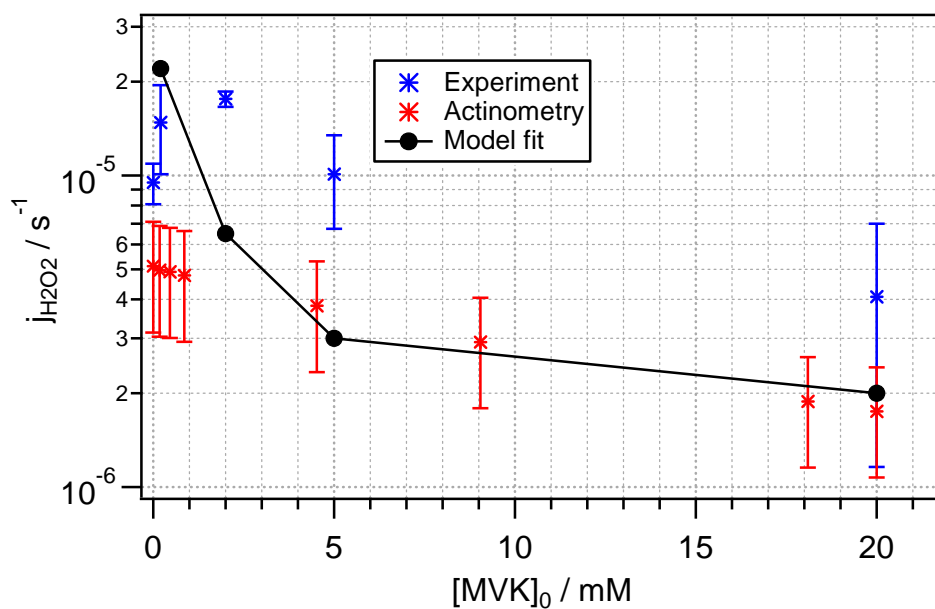


Figure 2: Comparison of experimental and model results using the mechanism listed in Table 1 and $j_{H_2O_2}$ in Figure 3 for four initial MVK concentrations (a) ~20 mM (fit to two experiments); (b) ~5 mM; (c) ~2 mM; (d) ~0.2 mM. (e) $[MVK]_0 = 20 \text{ mM}$; low oxygen concentration.



1

2

3 **Figure 3.** Experimentally determined photolysis rates for H₂O₂ (blue), and calculated data
 4 based on actinometry (red) using Eqs. 1 and 2, as a function of MVK initial concentration (left
 5 axis). Photolysis rate constants, fitted by the model in order to match MVK decay profiles for
 6 experiments with different initial MVK concentrations (black).

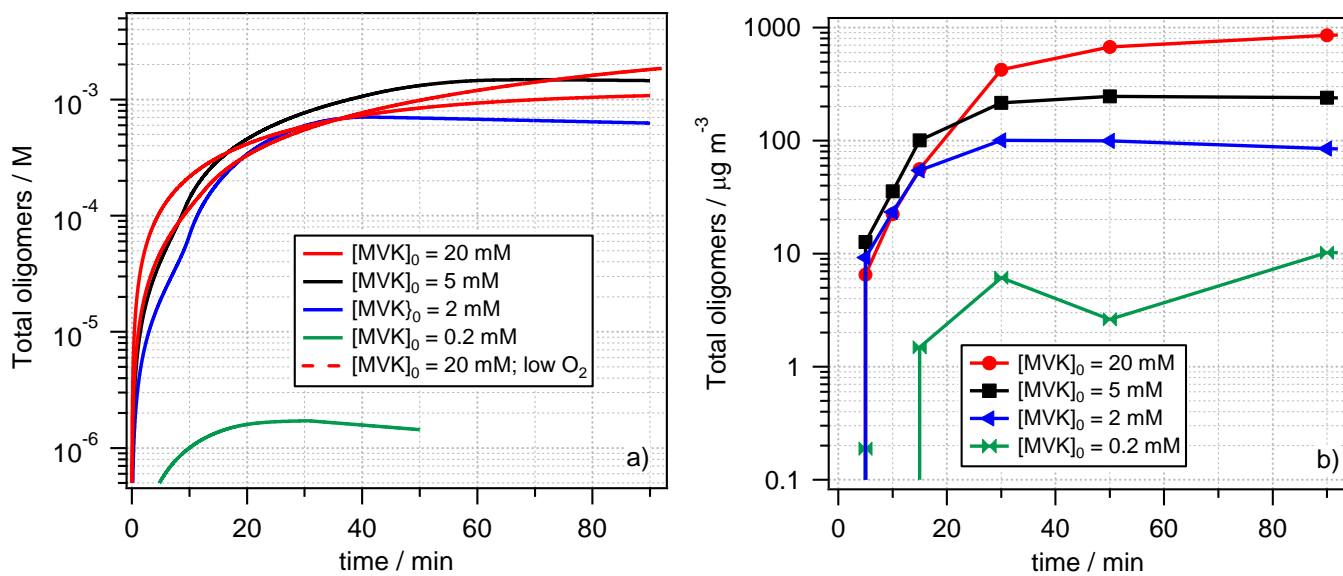


Figure 4. (a) Predicted oligomer concentrations (sum of all 6 oligomer series in Figure 1) for different initial MVK concentrations (constant $[\text{MVK}]_0 / [\text{H}_2\text{O}_2]_0$)

(b) Total oligomer mass, determined by SMPS measurements from the nebulized solutions (cf Figure 7 by Renard et al., 2015 (*Part I*)).

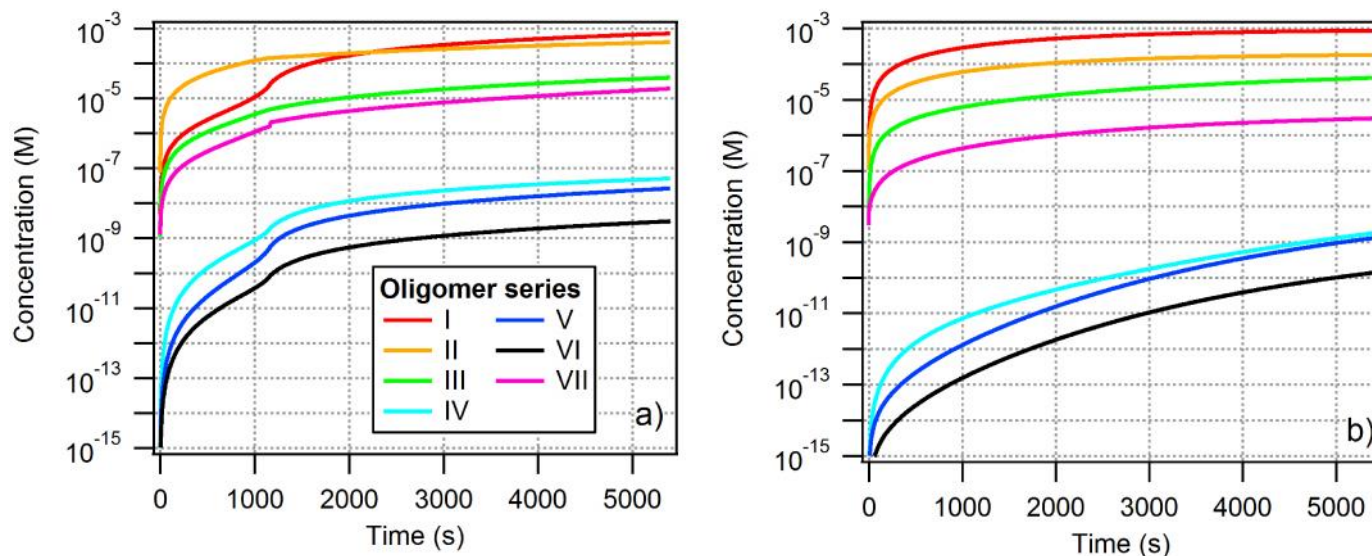


Figure 5. Comparison of predicted evolution for individual oligomer series I – VII (Figure 1) for $[MVK]_0 = 20$ mM for (a) high (saturated) and (b) low initial oxygen concentrations.

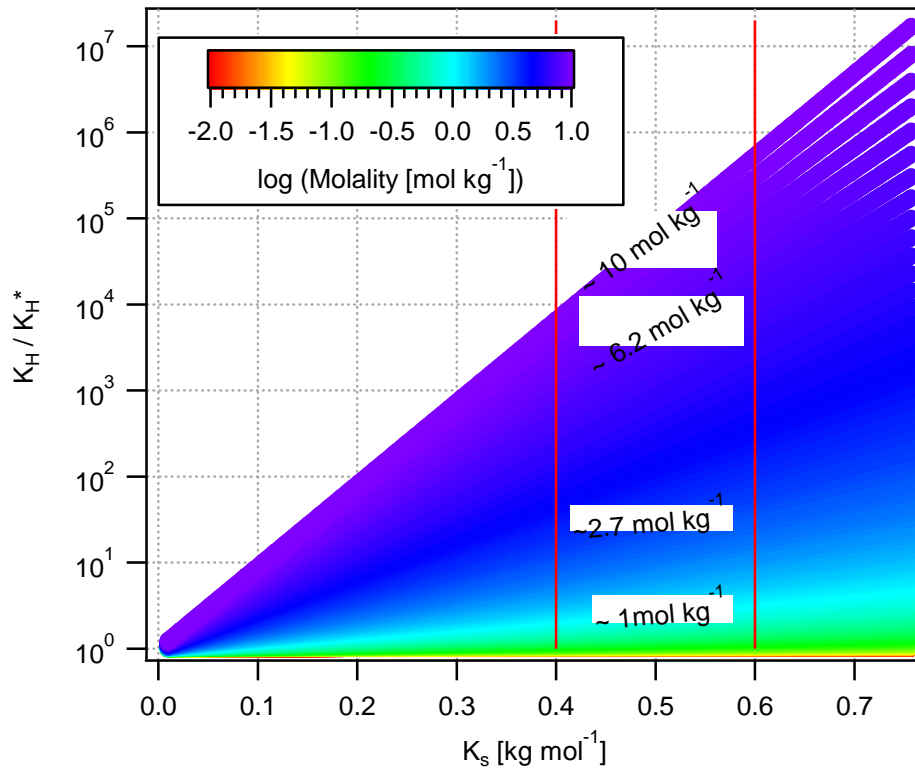


Figure 6: Reduction of solubility due to ionic strength (K_H/K_H^*) as a function of Setchenov coefficient K_s according to Equation 4. The vertical lines show the approximate range of K_s values for ketones (Wang et al., 2014). Molalities of $\sim 2.7 \text{ mol kg}^{-1}$ and $\sim 6.2 \text{ mol kg}^{-1}$ refer to saturated ammonium sulfate and sodium chloride solutions, respectively.

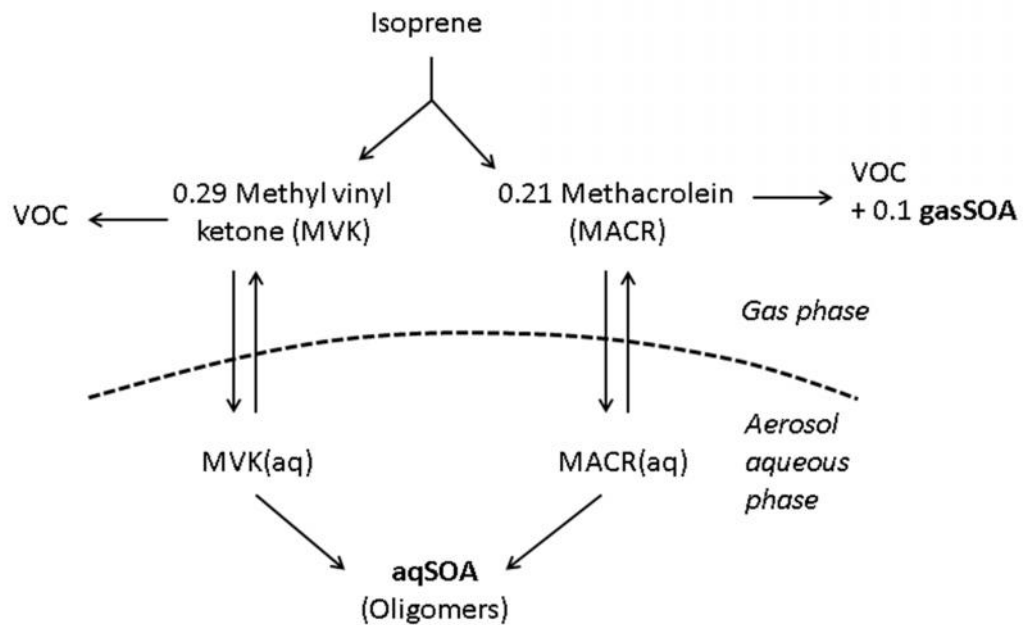


Figure 7. Schematic of SOA formation from isoprene in the atmospheric multiphase system; parameters for all processes are summarized in Tables 1-3.

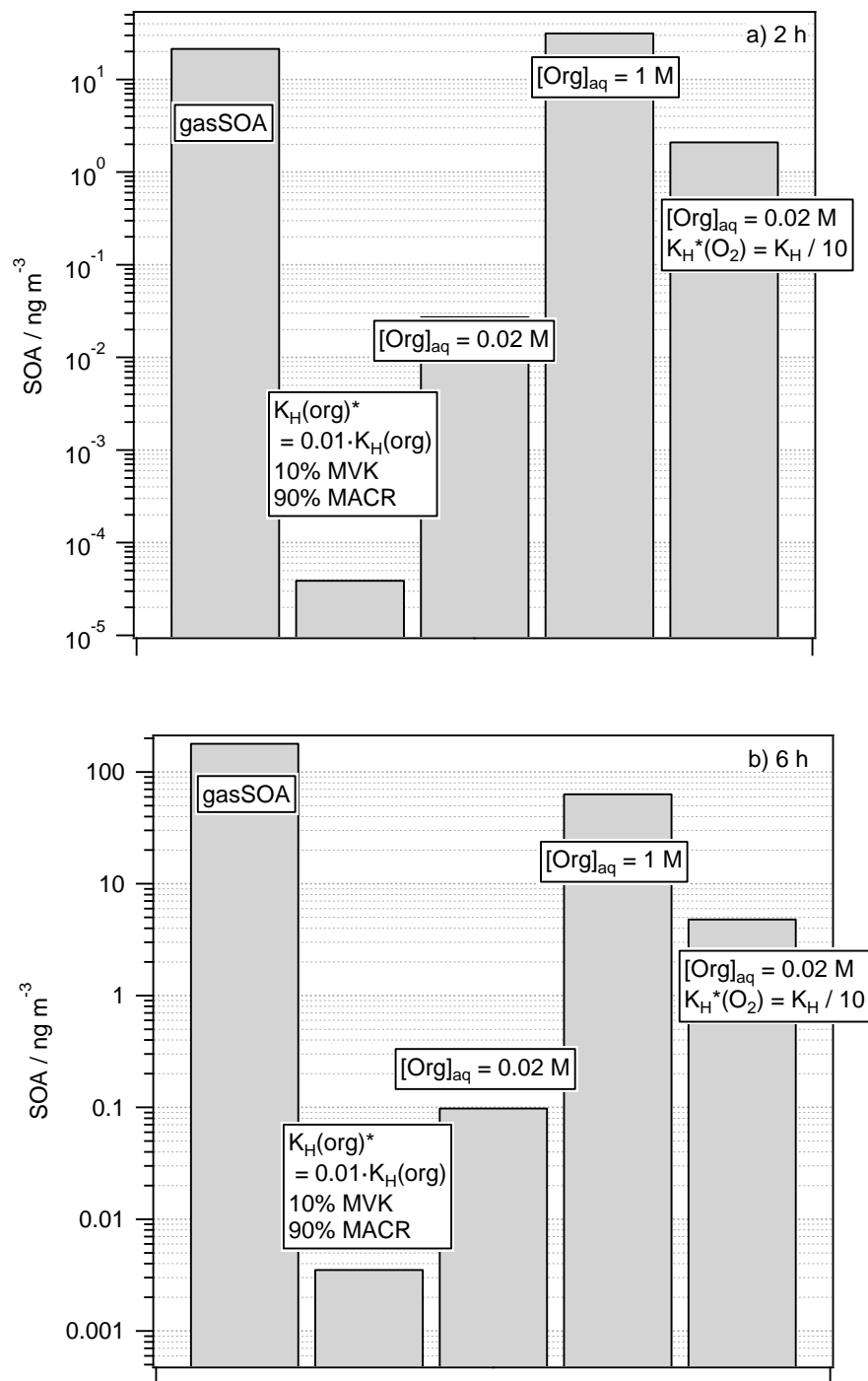


Figure 8. Comparison of gasSOA (1st bar) and aqSOA formation. Different assumptions are made for the solubility and total concentration of oligomer precursors in the aqueous phase: Reduced solubility of MVK and MACR due to ionic strength effects (2nd bar); different aqueous concentration of potential oligomer precursors (2nd, 3rd bar); and additionally reduced solubility of oxygen due to ionic strength effects.